



Satellite maneuver detection and estimation with optical survey observations

Alejandro Pastor^{1,2}  · Guillermo Escribano² · Manuel Sanjurjo-Rivo² · Diego Escobar¹

Accepted: 7 February 2022 / Published online: 7 June 2022
© The Author(s) 2022

Abstract

Maneuver detection and estimation is deemed crucial for maintaining catalogs of Resident Space Objects (RSOs) as it helps to avoid sets of duplicated objects and track correlation issues. In fact, maneuvers, along with launches and break-up events, are the main source of potential new object detections during RSOs cataloging activities. For the continuous and reliable provision of Space Situational Awareness (SSA) and Space Traffic Management (STM) services, a challenging trade-off between detection time and characterization accuracy of maneuvers needs to be performed. In this paper, two novel and operationally feasible methodologies are proposed for maneuver detection and estimation. The first, a track-to-orbit methodology, uses a pre-maneuver orbit to linearize the dynamics and estimate the single burn that minimizes the residuals of the post-maneuver tracks. The second, an orbit-to-orbit methodology, estimates the double burn that solves a minimization problem between the pre-maneuver and post-maneuver orbits. Both methods, based on an optimal control approach, are not only proposed to tackle the maneuver estimation problem but also to be integrated on operational and robust association frameworks. Results are presented for optical scenarios with both simulated and real data, providing insightful conclusions on the capabilities, performance and limitations of the proposed methods. Particular emphasis is given to the importance of the track association, since a single track is usually not enough to perform a reliable estimation of the maneuver. Besides, the capability of the methods to provide a solution to the association problem, even when not perfectly characterizing the true maneuver, is discussed.

Keywords Maneuver estimation · Maneuver detection · Track-to-orbit · Orbit-to-orbit · Optical observations

This article belongs to the Topical Collection:
Advanced Maui Optical and Space Surveillance Technologies (AMOS 2020)
Guest Editors: James M. Frith, Lauchie Scott and Islam Hussein

Extended author information available on the last page of the article

1 Introduction

The increasing number of Resident Space Objects (RSOs) and congestion of the orbital debris environment renders the space cataloging activities more challenging year after year. Currently, there are over 500 operational satellites only in Geostationary Earth Orbit (GEO) [1], most of which perform maneuvers every one or two weeks and for which Space Surveillance and Tracking (SST) systems predominantly have optical observations.

The main issue for SST systems related to maneuvering RSOs is the challenging correlation of observations. In the case of survey sensors, correlation is usually performed by comparing real and simulated observations, generated from predicted orbits of already cataloged RSOs. Unless these predicted orbits take into account the maneuver plan followed by the operators, correlation analysis of the first track after a maneuver will fail for sufficiently large magnitude maneuvers and after enough time to impact the orbit. Even for tracking sensors this is a problem, since the RSOs might not be located where expected, therefore leading to an observability issue. This may result in a loss of the RSO or ambiguous correlation situations, where the identity of the observed object is not clear. In those cases, although the correlation could be achieved, maneuver estimation is still required to properly update the state of the RSO through orbit determination. In fact, maneuvers represent currently the primary contribution to potential new detections (more than 500 operational satellites only in GEO [2], most of which perform maneuvers every one or two weeks in the case of chemical propulsion or even daily in the case of electric propulsion), exceeding those related to satellite launches (less than 400 spacecraft launched per year [2]) and break-up events (less than ten events per year, 98% of which involves less than 300 debris cataloged [3]), so detecting them is crucial for maintaining catalogs of RSOs. Capable maneuver detection and estimation methods are a must since otherwise these potential new detections would be promoted to actual new objects leading to sets of duplicated RSOs, thereby polluting the catalog and hampering the provision of Space Situational Awareness (SSA) and Space Traffic Management (STM) services.

At this point it may be convenient to clarify some terms that are extensively used along this paper and whose definitions may depend on the particular field of study. On the one hand, we use the term *track* to refer to a set of observations taken by a single sensor usually over a short time period, originated from the same RSO and frequently not enough to reliably estimate an orbit. Tracks (or tracklets) obtained from optical and radar surveillance sensors are usually referred to as uncorrelated optical observations (UCOs) and uncorrelated tracks (UCTs) when they cannot be associated to any cataloged RSO, respectively. We will refer to them as tracks, regardless of the sensor type. On the other hand, a well-established estimation of the trajectory of an RSO in the catalog is called *orbit*. Accordingly, we refer to *track-to-track* (T2T), *track-to-orbit* (T2O) and *orbit-to-orbit* (O2O) as the association or correlation of tracks, tracks and orbits, and orbits, respectively.

Maneuver detection and estimation can be tackled as part of the association or correlation problem and should be integrated within the cataloging chain

herein used, as depicted in Fig. 1, which shows a view of the different processes involved. This paper focuses on two methods for maneuver detection and estimation (located inside branches 1 and 2). In order to update the cataloged orbits and solve the T2O and O2O association problems, these two methods must be integrated in an association framework. The very first UCT received after a maneuver will most likely not be reliably correlated against any RSO in the catalog due to the velocity change and its effects on the dynamics, so it enters into the T2T association algorithm, intended for the detection of new objects. Initially, this first post-maneuver UCT cannot be associated to any other track in the T2T process. However, as more post-maneuver UCTs are obtained, these can be associated. If nothing is done to detect the maneuvers, the set of correlated tracks would coalesce in a new object. In order to prevent this, depending on the complexity of the maneuver, two main possibilities arise (branches 1 and 2 in Fig. 1):

- **Maneuver detection and estimation from uncorrelated tracks:** the new UCT is first associated with the corresponding orbit of the RSO via T2O correlation considering a single-burn maneuver (branch 1 in Fig. 1). This allows to establish a first and preliminary link - association or hypothesis in the Multiple Hypothesis Tracking (MHT) framework - between an orbit and a single UCT, although the maneuver cannot be yet confirmed nor estimated reliably due to the scarce information available. It is important to note that not every RSO in the catalog is considered, but only a subset of candidates, such as those identified as active satellites that have not been recently updated. The maneuver detection and estimation should be performed in the observations space by means of a T2O methodology including maneuvers as described below. The rationale behind this is that the orbital estimation derived from the new UCT (or the few associated UCTs) is still not reliable enough to be directly used. As more UCTs after the maneuver become available to the system, new associations of more tracks arise until there

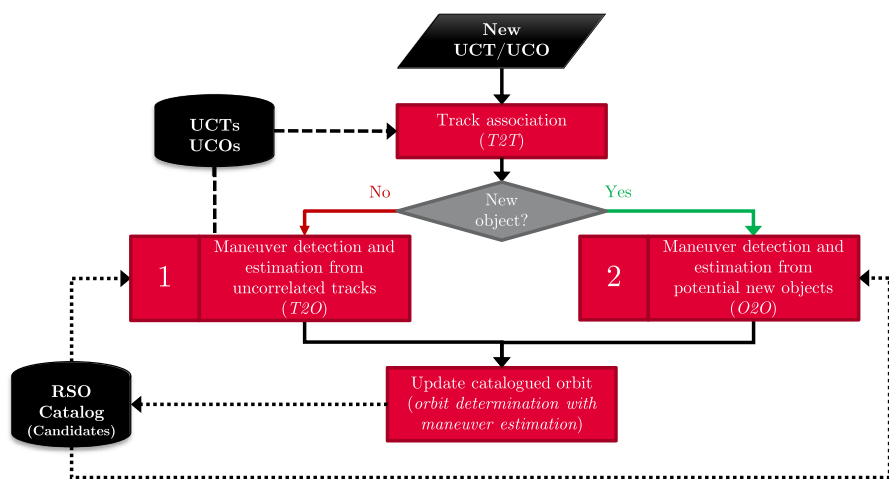


Fig. 1 Maneuver detection and estimation role in the cataloging chain

is enough information to promote, i.e. confirm, the hypothesized maneuver. The number of tracks for the association required to properly confirm and estimate a single burn maneuver (i.e., promote a hypotheses) is expected to be around two or three, as suggested in [4]. In any case, less than the four required for a full and nominal RSO initialization in the catalog [5, 6]. The proposed T2O methodology is able to estimate maneuvers based on residuals between the estimated orbit before the maneuver and observations afterwards. Figure 2 shows the residuals of observations from four telescopes of the International Scientific Optical Network (ISON) and a GEO satellite before and after a North-South maneuver (vertical dashed line). The more time after the maneuver elapses, the greater the divergence of the residuals. This is an indication of the footprint of the maneuver on the residuals of the post-maneuver tracks when considering the pre-maneuver orbit.

- **Maneuver detection and estimation from potential new object:** the information contained on a small number of tracks might not be enough to estimate the parameters characterizing a maneuver of two burns, since the T2O methodology (branch 1 in Fig. 1) would not be able to associate the orbit with the post-maneuver UCTs. Therefore, it is required to associate a higher number of post-maneuver tracks to obtain a new and reliable orbit estimation without the use of prior information, i.e. perform a potential new RSO detection by means of T2T association. The number of tracks required is greater than in the previous situation, since a full RSO initialization needs to be performed. Once accurate post-maneuver orbital information is available, the maneuver detection and estimation can be done in the orbit space by means of an O2O methodology considering maneuvers (branch 2 in Fig. 1). This problem corresponds to the estimation of two maneuvers capable of linking two already well-established orbits. The case of low-thrust maneuvers may pose challenges to this approach. Nonetheless, the methodology is expected to remain applicable as long as the low-thrust maneu-

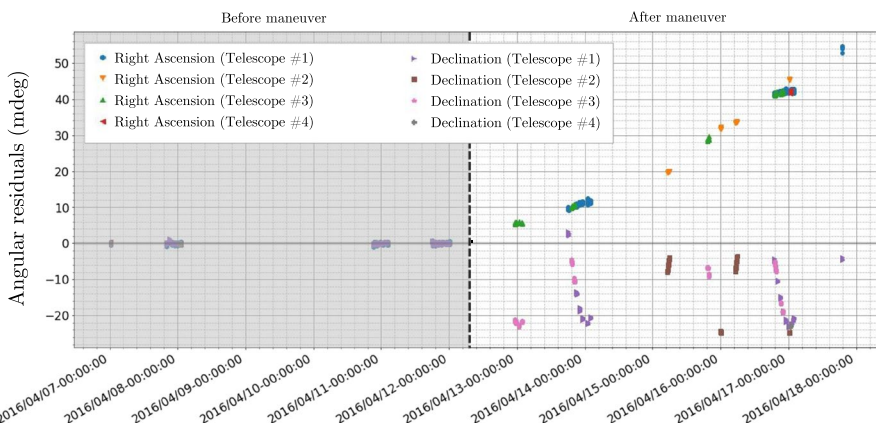


Fig. 2 Residuals between the estimated orbit before the maneuver and measurements after the maneuver

ver has finished, although the estimated impulsive burns would not be very representative of the actual low-thrust maneuver performed.

Multi Target Tracking (MTT) methods, traditionally applied to sensing, guidance, navigation and air traffic control, among others [7], have been also used to tackle the T2T association problem. One can find the work of Stauch et al. [8] based on Joint Probabilistic Data Association (JPDA) [9] and Constrained Admissible Regions (CAR) [10], and the one by Pirovano et al. [11], still based on JPDA and CAR but with a different treatment for the uncertainty following Differential Algebra (DA). JPDA consists in the joint association of objects and observations disregarding the one-to-one association constraint, thus alleviating the decision-making process. Alternatively, Aristoff et al. [12] propose a MHT approach, in which only one-to-one associations are allowed, yet maintaining multiple parallel hypotheses to be tested as new observations arrive. Jones and Vo [13] suggest utilizing a purely statistical framework for RSO catalog maintenance based on Random Finite Sets (RFSs), thus accommodating uncertainty in the number of objects. Beside decision making and statistical association methods, Siminski et al. [14] discuss on the particular application to GEO objects and optical observations. Finally, Furfaro et al. [15] apply machine learning methods to study the variability in space object catalogs and identify feasible trends. However, none of these methods is capable of dealing with maneuvering objects, which may lead to object duplication or false associations if the maneuver exceeds the association uncertainty or likelihood.

The automatic detection of maneuvering RSOs can be framed within the general multi-target tracking-association problem, in which the tracked objects are allowed to maneuver. Some approaches [16, 17] take digested information from Two Line Elements (TLEs) to isolate, and thus detect, maneuver intervals. Moreover, a proper treatment of historical data may be used to integrate maneuver detection capabilities within the association problem, i.e. in an on-line fashion. In this regard, Siminski et al. [18] present an implementation based on actual maneuver data reported by the operator, which employs a kernel density estimator to cluster maneuverers of different nature and define admissible regions. Alternatively, Shabarekh et al. [19] developed a machine learning approach aimed at determining the Patterns of Life (PoL) in order to predict and characterize maneuvers. In fact, these techniques [18, 19] can be readily integrated in an operational framework as they are devised to inherit real measurement data.

Maneuver estimation has also been assessed by means of optimal control methods. For instance, Holzinger and Scheeres [20] and Holzinger et al. [21] developed an alternative method to JPDA based on distance control metrics as opposed to the usual Mahalanobis distance [22], which is aimed at determining the minimum required control effort to fit a given observation. On the same topic, Lubey [23] emphasizes on the ability to jointly consider maneuver detection and data association, contributing with a thorough uncertainty characterization. These methods characterize the maneuver as a continuous perturbing acceleration of varying magnitude, whereas an impulsive-based approach may also be embraced. The work in [24, 25] suggests utilizing the concept of the state transition matrix

to evaluate the impact of an impulsive maneuver in the form of a perturbation. A minimization problem can then be formulated in order to derive the parameters defining the maneuver. Note however, the authors only consider an O2O scenario and use a simplified maneuver model: either one or two burns in the direction of the orbital velocity. An extension to [24, 25] is the work by Yang et al. [26], which discuss on the uncertainty propagation of maneuvering objects by means of state transition tensors of order four, as opposed to the first order approach based on the use of transition matrices. However, this first order approach has proved to be accurate enough to estimate large and small maneuvers [4, 27] and have been also applied to relative motion dynamics [28].

Most of the aforementioned methods must be tested and tuned for each specific application. The characteristics of the maneuver detection and estimation problem, especially considering scarcity of data and large time intervals between tracks makes the tuning demanding. In previous years, a series of works have tried to address the gaps of the classical approaches with methods developed ad-hoc for the SST problem [18, 23, 27]. In those works, RSO maneuvers are characterized a-priori, in order to incorporate more information to the problem, and make it more tractable. Alternatively, thrust Fourier coefficients have been used to estimate equivalent maneuvers with the same secular behavior and without the need of any a-priori information [29]. Nevertheless, most of them provide results for particular and isolated test cases, rather than representative enough scenarios, analogous to an operational SST system. Scalability concerns, as in the track association problem [5], is of a major importance, given the dimensions of the problem and the huge number of a-priori possible combinations to evaluate.

To address the above-mentioned gaps, we propose two maneuver detection and estimation methods to be used in operational and robust cataloging chains. They do not require any a-priori information of the maneuver and are able to provide an estimation to update the cataloged orbit of the involved RSO. To do so, uncorrelated tracks are associated among them (T2T) and then cataloged orbits are correlated against these post-maneuver track associations (T2O including candidate maneuvers of both single and double burns). In this way, associations of orbits and tracks, or hypotheses, are generated, scored, pruned and promoted in such a way that the involved cataloged orbit and sensing data belongs to a common maneuvered RSO. For instance, maneuvers involving excessive control effort are discarded since they are not realistic but solutions to the orbit linkage problem. Note that in this case the maneuver detection and track correlation problem are coupled. Solving this coupled problem yields both the object identification for which the sensor data is generated as well as the maneuver time, direction and size. This would allow to considerably reduce the maneuver detection time, since T2O association, as opposed to O2O, does not require a new object detection and initiation. However, an alternative formulation is proposed to consider O2O correlation scenarios in which two established objects may be reduced to a single maneuvered one. Opposed to the single impulsive burn of the T2O correlation, this last O2O scenario assumes a double impulsive burn to allow for a transfer orbit capable of approximating maneuvers in a more robust manner.

The present paper is structured in five sections. Section 1 has introduced the role of maneuver detection and estimation on cataloging activities, a state-of-the-art review and the framework of our methodologies. Sections 2 and 3 present the T2O and O2O methodologies for single and double burns maneuver estimation, respectively. Section 4 shows and analyzes the results with both simulated and real observations. Finally, Section 5 gathers the conclusions of the paper and discusses the current status of the work.

2 Single burn maneuver detection and estimation via T2O

The T2O methodology is proposed to solve the maneuver detection and estimation problem when a pre-maneuver orbit and post-maneuver tracks are available. On the one hand, we assume a pre-maneuver orbit (subscript A), an orbit estimated before the maneuver, is available on the catalog. This means that an extended state vector:

$$y_A(t) = [x_A(t), p_A]^T \in \mathbb{R}^{6+n_p} \tag{1}$$

is given, where $x_A(t) = [r_A(t), v_A(t)]^T \in \mathbb{R}^6$ and $p_A \in \mathbb{R}^{n_p}$ represent the state vector and dynamical parameters, respectively, being $r_A \in \mathbb{R}^3$ and $v_A \in \mathbb{R}^3$ the corresponding position and velocity vectors.

On the other hand, a set of N optical observations, $z(t_i) \in \mathbb{R}^2$ for $i = 1, \dots, N$, has been received by the sensor network. Each observation contains a pair of right ascension and declination measurements referred to t_i , packed in tracks so that each track contains only observations from a common sensor over a short time period. These N observations may come from $n_T \leq N$ optical tracks, which shall have been previously associated with other methods, such as the association framework presented in [5].

The maneuver can be detected by inspection of the residuals of the post-maneuver tracks and the pre-maneuver orbit (see Fig. 2). The divergence of the residuals can be found by setting a threshold on the residuals weighted with the expected measurement noise of the involved sensor. In this way, the maneuver detection and estimation is triggered whenever absolute or relative threshold criteria are met.

Let $\Psi(t, t_0)$ be the full transition matrix, allowing to propagate perturbations of the extended state vector from t_0 to t under the linear dynamics assumption, i.e.:

$$\Psi(t, t_0) = \frac{\partial x(t)}{\partial y(t_0)} \in \mathbb{R}^6 \times \mathbb{R}^{6+n_p} \tag{2}$$

Note that $\Psi(t, t_0)$ contains the so-called state transition, and sensitivity matrices [30]:

$$\Phi(t, t_0) = \partial x(t) / \partial x(t_0) \in \mathbb{R}^6 \times \mathbb{R}^6 \tag{3}$$

$$S(t, t_0) = \partial x(t) / \partial p \in \mathbb{R}^6 \times \mathbb{R}^{n_p} \tag{4}$$

Subsets of these matrices will be referred to as $(\cdot)_{\alpha\beta}$, corresponding to $\partial\alpha(t)/\partial\beta(t_0)$.

At a certain epoch, t_M , an impulsive maneuver takes place causing a sudden change in the velocity, i.e.: $\mathbf{u} = \mathbf{v}_B(t_M) - \mathbf{v}_A(t_M)$, as shown in Fig. 3. Since the position of the two orbits is intersecting at t_M , i.e.: $\mathbf{r}_A(t_M) = \mathbf{r}_B(t_M)$, the post-maneuver state (subscript B) can be obtained by considering the maneuver a perturbation at time t_i as follows:

$$\mathbf{x}_B(t) = \mathbf{x}_A(t) + \Psi_{xv}(t, t_M)\mathbf{u} \tag{5}$$

Then, the maneuver magnitude, $\mathbf{u} \in \mathbb{R}^3$, for a given t_M , is estimated so that the residuals of the observations, $\rho_i = z(t_i) - \mathbf{h}(t_i, \mathbf{y}(t_i))$, difference between actual measurements and measurements reconstructed from the post-maneuver orbit, perturbed with the solve-for maneuver, is minimized, i.e.:

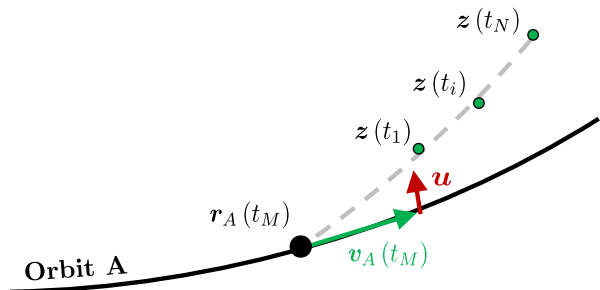
$$J = \frac{1}{N} \sum_{i=1}^N \rho_i^T \mathbf{W}_i \rho_i \tag{6}$$

being \mathbf{W} the weighting matrix, which contains the inverse of the expected variance of each measurement. The solution can be obtained via a weighted non-linear least-squares method. To do so, the problem is linearized around a reference point, \mathbf{u}_0 , and the corresponding correction, $\Delta\mathbf{u}$, is obtained by solving the following linear system:

$$(\mathbf{G}^T \mathbf{W} \mathbf{G}) \Delta\mathbf{u} = (\mathbf{G}^T \mathbf{W}) \Delta\mathbf{z} \tag{7}$$

where \mathbf{G} is the Jacobian, i.e.: partials of the measurements with respect to the estimated parameters, and $\Delta\mathbf{z}$ is the difference between the actual observations and the observations predicted from the reference trajectory. This expression is similar to the classical orbit determination problem: $(\mathbf{H}^T \mathbf{W} \mathbf{H}) \Delta\mathbf{y} = (\mathbf{H}^T \mathbf{W}) \Delta\mathbf{z}$ [30], in which the residuals are minimized, being \mathbf{H} the Jacobian with respect to the state vector in this case (partials of the measurements with respect to the state vector). In the problem at hand the Jacobian \mathbf{G} is computed with respect to the parameters of the single burn maneuver \mathbf{u} as opposed to \mathbf{y} in \mathbf{H} .

Fig. 3 Sketch of the proposed T2O maneuver estimation problem



Note that the state vector at each observation epoch, corresponding to the post-maneuver orbit and required for the evaluation of the Jacobian and residuals, can be linearly propagated by means of Eq. 5.

Starting from a null initial solution and iteratively solving Eq. 7 it is possible to obtain an estimation for Δu . The Jacobian should be updated at each iteration to ensure convergence. Then, the contribution to G of the i^{th} observation is:

$$G_i = \frac{\partial h(t_i, y_B(t_i))}{\partial u} = \frac{\partial h(t_i, y_B(t_i))}{\partial x_B(t_i)} \frac{\partial x_B(t_i)}{\partial v_B(t_M)} \frac{\partial v_B(t_M)}{\partial u} = H_i \Psi_{xv}(t_i, t_M) \quad (8)$$

In order to detect the maneuver, the least-squares problem must be solved for a range of t_M values. In principle, the maneuver is assumed to have occurred after t_A^+ , the epoch of the last observation considered for the estimation of the pre-maneuver orbit, and t_1 , the epoch of the first available new observation. This thus makes it desirable to have a very computationally efficient estimation method, which is the rationale behind using a linearized post-maneuver orbit propagation, rather than a fully numerical one.

Finally, a set of estimations $\{u_k\}$ and corresponding objective function values $\{J_k\}$ for each $t_k \in \mathcal{T}$ for which the problem could be solved are to be obtained. Since the final goal of the maneuver estimation problem presented is the T2O association, we suggest taking every local minima of J and then selecting the solution as the one leading to minimum $|u|$ (where $|\cdot|$ denotes the Euclidean norm when applied to a vector). Additional constraints can be included, such as introducing a u_{max} value to avoid the consideration of unrealistic maneuvers. Moreover, the n solutions leading to minimum $|u|$ can be retained for a MHT approach. Note that the methodology provides a set of compatible solutions and their corresponding score (i.e. maneuver magnitude), and as such can be readily integrated in an association framework to solve the T2O correlation problem. The complete method is summarized in Algorithm 1, where $\hat{\cdot}$ denotes estimated values.

Algorithm 1 T2O methodology.

Require: y_A and z_i for $i = 1, \dots, N$

- 1: **for** $t_M \in \mathcal{T} = [t_A^+, t_1]$ **do** ▷ Loop on maneuver epoch
 - 2: Initial solution: $u = \mathbf{0}$
 - 3: Estimate u that minimizes the residuals (Eq.7)
 - 4: **end for**
 - 5: Locate J local minima in \mathcal{T}
 - 6: Discard solutions with $|\hat{u}| > u_{max}$
 - 7: Sort remaining solutions according to $|\hat{u}|$
-

3 Double burn maneuver detection and estimation via O2O

The O2O methodology is proposed to solve the maneuver estimation problem when a pre-maneuver and post-maneuver orbits are available. In this case, we assume both the pre-maneuver orbit, y_A , and the post-maneuver orbit, y_B , are given. The

estimation process can be triggered when a residuals divergence is identified, analogously as in Section 2. Besides, this methodology should be applied before publishing the second orbit in the catalog to avoid duplicated objects.

The problem is then to find the transfer orbit, \mathbf{x}_T , that connects the pre-maneuver and post-maneuver orbits, i.e.:

$$\begin{cases} \mathbf{0} &= \mathbf{r}_T(t_{M1}) - \mathbf{r}_A(t_{M1}) \\ \mathbf{u}_1 &= \mathbf{v}_T(t_{M1}) - \mathbf{v}_A(t_{M1}) \end{cases} \tag{9}$$

$$\begin{cases} \mathbf{0} &= \mathbf{r}_B(t_{M2}) - \mathbf{r}_T(t_{M2}) \\ \mathbf{u}_2 &= \mathbf{v}_B(t_{M2}) - \mathbf{v}_T(t_{M2}) \end{cases} \tag{10}$$

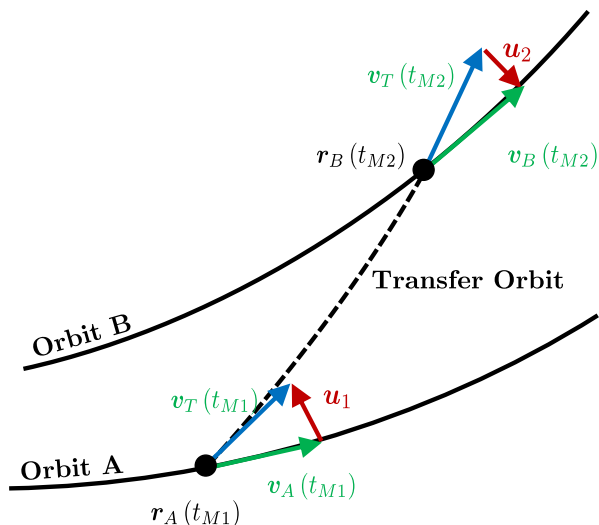
where \mathbf{u}_i represents the i^{th} burn, i.e., delta-V, to be estimated.

The problem, illustrated in Fig. 4 can be solved for $t_{M1}, t_{M2} \in \mathcal{T}$ such that $t_A^+ < t_{M1}$ (i.e.: the first burn occurs after the last observation used in the estimation of the pre-maneuver orbit) and $t_{M1} < t_{M2} < t_B^-$ (i.e., the second burn takes place after the first burn and prior to the first observation used in the estimation of the post-maneuver orbit).

Although the solution could be determined by solving Lambert’s problem between $\mathbf{r}_A(t_{M1})$ and $\mathbf{r}_B(t_{M2})$ and then recovering the maneuver magnitudes directly from Eqs. 9 and 10, we propose a method that uses linearized dynamics to propagate the effect of the maneuvers (as perturbations) in the orbits. This way, we avoid the limitation of the two-body motion dynamical model (i.e. Kepler’s law) by considering relevant perturbations while keeping the computational effort low. Two equations arise from the propagation of the pre-maneuver and post-maneuver orbits, respectively:

$$\mathbf{x}_T(t) = \mathbf{x}_A(t) + \Phi_{A,xv}(t, t_{M1})\mathbf{u}_1 \tag{11}$$

Fig. 4 Sketch of the proposed O2O maneuver estimation problem



$$\mathbf{x}_T(t) = \mathbf{x}_B(t) - \Phi_{B,xv}(t, t_{M2})\mathbf{u}_2 \tag{12}$$

A determined linear system can be constructed by using the linearized dynamics of the pre-maneuver orbit (A):

$$\begin{bmatrix} \mathbf{A}_{rv} & \mathbf{0} \\ \mathbf{A}_{vv} & \mathbf{I} \end{bmatrix} \cdot \begin{Bmatrix} \mathbf{u}_1 \\ \mathbf{u}_2 \end{Bmatrix} = \begin{Bmatrix} \Delta_{2,r} \\ \Delta_{2,v} \end{Bmatrix} \tag{13}$$

with:

$$\mathbf{A}_{\alpha\beta} = \frac{\partial \alpha_A(t_{M2})}{\partial \beta_A(t_{M1})} = \Phi_{A,\alpha\beta}(t_{M2}, t_{M1}) \tag{14}$$

$$\Delta_{k,\alpha} = \alpha_B(t_{Mk}) - \alpha_A(t_{Mk}) \tag{15}$$

Analogously, a determined linear system can be constructed by using the linearized dynamics of the post-maneuver orbit (B):

$$\begin{bmatrix} \mathbf{0} & \mathbf{B}_{rv} \\ \mathbf{I} & \mathbf{B}_{vv} \end{bmatrix} \cdot \begin{Bmatrix} \mathbf{u}_1 \\ \mathbf{u}_2 \end{Bmatrix} = \begin{Bmatrix} \Delta_{1,r} \\ \Delta_{1,v} \end{Bmatrix} \tag{16}$$

with:

$$\mathbf{B}_{\alpha\beta} = \frac{\partial \alpha_B(t_{M1})}{\partial \beta_B(t_{M2})} = \Phi_{B,\alpha\beta}(t_{M1}, t_{M2}) \tag{17}$$

Although either Eqs. 13 or 16 could be directly solved to obtain \mathbf{u}_1 and \mathbf{u}_2 , we suggest combining the two linear systems to obtain the following problem:

$$\begin{bmatrix} \mathbf{0} & \mathbf{B}_{rv} \\ \mathbf{I} & \mathbf{B}_{vv} \\ \mathbf{A}_{rv} & \mathbf{0} \\ \mathbf{A}_{vv} & \mathbf{I} \end{bmatrix} \cdot \begin{Bmatrix} \mathbf{u}_1 \\ \mathbf{u}_2 \end{Bmatrix} = \begin{Bmatrix} \Delta_{1,r} \\ \Delta_{1,v} \\ \Delta_{2,r} \\ \Delta_{2,v} \end{Bmatrix} \tag{18}$$

The solution of this overdetermined system (12 equations, 6 unknowns) can be obtained via least-squares, i.e., by solving the following linear system:

$$(\mathbf{X}^T \mathbf{X})\mathbf{u} = \mathbf{X}^T \Delta \tag{19}$$

where \mathbf{X} is the left-hand-side matrix and Δ the right-hand-side vector in Eq. 18. $\mathbf{u} = \{\mathbf{u}_1, \mathbf{u}_2\}^T$ can be solved with any factorization method such as Cholesky decomposition.

Since this method is based on a linearization of the dynamics of the two orbits, there is an inherent applicability limitation related to the magnitude of the perturbations above which the linear dynamics assumption is expected to fail.

The solution of Eq. 18 is expected to be a smooth combination of the two dynamics. Moreover, note that the contribution of each orbit could be weighted if required

with a confidence level or covariance, for instance. The complete method is summarized in Algorithm 2.

Algorithm 2 O2O methodology.

Require: y_A and y_B

- 1: **for** $t_{M1}, t_{M2} \in \mathcal{T} = [t_A^+, t_{M2}] \times [t_{M1}, t_B^-]$ **do** ▷ Loop on maneuver epoch
 - 2: Solve overdetermined linear problem (Eq.18)
 - 3: **end for**
 - 4: Discard solutions with $|\hat{u}| > u_{max}$
 - 5: Sort remaining solutions according to $|\hat{u}|$
-

4 Results

The T2O and O2O methods, presented in Sections 2 and 3, have been applied to scenarios with simulated and real observations of GEO RSOs. These scenarios are briefly introduced next:

- *Sat#0* (simulated scenario): a series of impulsive burns, intended to validate and evaluate the performance of the methodologies under a controlled scenario.
- *Sat#1* (real scenario): impulsive Station Keeping (SK) burns, both North-South (NS) and East-West (EW), representative of typical maneuvers performed by GEO satellites.
- *Sat#2* (real scenario): impulsive EW SK burns, representative of typical maneuvers performed by GEO satellites.
- *Sat#3* (real scenario): impulsive re-orbiting maneuver of a satellite. This scenario intends to unveil potential limitations of the methodologies that may arise under large maneuvers.
- *Sat#4* (real scenario): maneuvers performed by a satellite equipped with electric propulsion. This scenario intends to study the performance of the methodologies when the impulsive maneuver hypothesis does not hold and the duration of the burn is of several hours.

The real scenarios use real observations from telescopes of the ISON sensor network covering maneuvers of GEO operational satellites used for communications and meteorological purposes (semi-major axis, eccentricity and inclination are included in Table 12 for reference). Besides, Figs. 27 and 28 present the distribution of the track duration (time between first and last observation of the track) and observation spacing (time between observations in a track) for all the tracks considered in the real scenarios. A total of 26 telescopes, listed in Table 13 and featuring a measurement error ranging from 0.5 to 1 arcsecond, have been considered in the analysis. Regarding the real maneuvers, reference values have been generated using additional external data (satellite operator maneuver plans and ranging observations with few meter-level errors on a post-maneuver orbit determination) and are considered as truth values.

Regarding the T2O methodology, the pre-maneuver orbit is estimated by using the observations available before the burn via a batch least-squares orbit determination and propagated to the future to cover the post-maneuver tracks. Then, the post-maneuver tracks are associated incrementally via T2T association [5]. Finally, the T2O method, presented in Section 2, is applied to each pair of pre-maneuver orbit and post-maneuver track association. A linear grid of maneuver epoch, t_M , values has been considered in all the results presented, with a time step of 1 hour in the simulated case (Sat#0), 15 minutes in the first real case (Sat#1) and 6 minutes in the rest of real cases (Sat#2, Sat#3 and Sat#4). The sequence of events is depicted in Fig. 5.

In the case of the O2O methodology, the pre-maneuver and post-maneuver orbits are estimated analogously, by means of an orbit determination with the observations available before and after the burns, respectively. Then, the O2O method, presented in Section 3, is applied to the pair of orbits. The sequence of events is depicted in Fig. 6.

The dynamical model considered for the state propagation, usual in the case of GEO RSOs, consists in a 30x30 Earth gravitational field, Moon and Sun third body perturbations and cannonball model for the Solar Radiation Pressure (SRP). Regarding the orbit determination, the state and the SRP coefficient are estimated.

Finally, the computational time of each case presented in this section is presented in Table 14. Note that in Sat#1, Sat#3 and Sat#4 scenarios the T2O methodology is applied to several associations of one, two, three and four tracks, so an average time is presented. Besides, the cases in which the T2O methodology is applied to all tracks (suffix A) is included for reference, but do not represent a typical case of application. The computational times correspond to single thread executions on a 2.60 GHz Intel(R) Xeon(R) Gold 6142 CPU.

4.1 Sat#0 scenario: simulated observations

The first scenario consists in a set of simulated single and double burn maneuvers, intended to validate the T2O and O2O methodologies, respectively. The involved

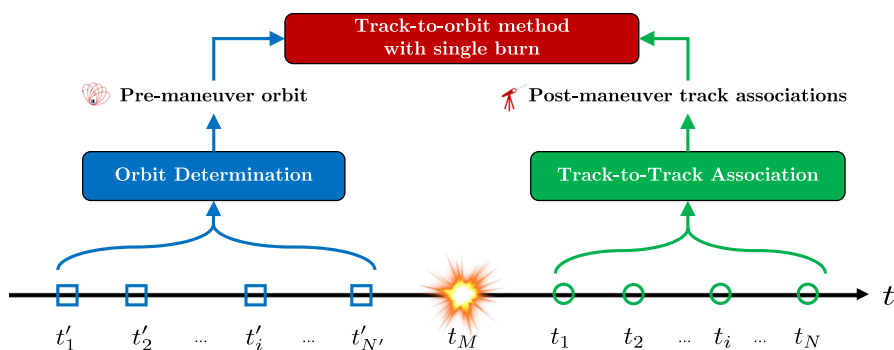


Fig. 5 Sequence of events for applying the T2O methodology

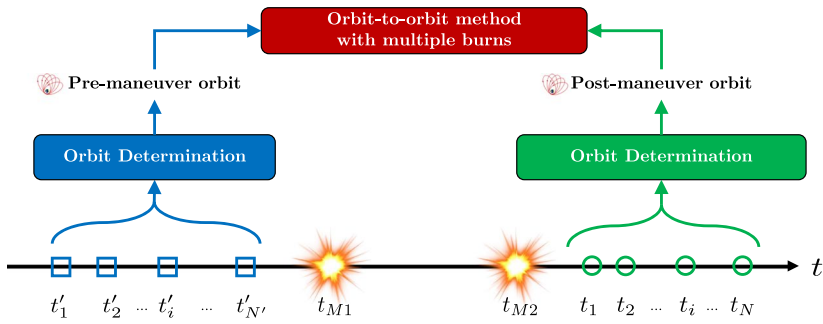


Fig. 6 Sequence of events for applying the O2O methodology

object, Sat#0, is located on a GEO orbit (see Table 1 for further details) and representative of a typical GEO satellite.

4.1.1 Single burns, T2O methodology

The first assessment of the T2O methodology is aimed at investigating the impact of the number of tracks and performing a preliminary analysis with the method under a simulated scenario. To do so, the initial state vector (Table 1) was propagated from t_0 up to $t_0 + 7$ days considering an impulsive burn in the local RIC frame (radial, in-track and cross-track) at the middle of the interval. Four cases have been studied: 1) radial burn, 2) in-track burn, 3) cross-track burn and 4) additional cross-track burn of high magnitude. The magnitude of the maneuvers is $|\mathbf{u}| = 1.0$ m/s for the three first cases and $|\mathbf{u}| = 10.0$ m/s for the last case.

On the one hand, a pre-maneuver orbit was estimated with simulated observations before the maneuver and propagated forward in time without considering the maneuver. On the other hand, an optical sensor station was simulated to generate three tracks on the 5th day (12 h after the maneuver), 6th day (36 h after the maneuver) and 7th day (60 h after the maneuver), according to the reference orbit. Each track has a duration of 15 min and contains one observation (pair of right ascension, α , and

Table 1 Sat#0 scenario: Initial state vector

Parameter	Value	Units
t_0	Day #1 at 00:00	
a	42,192.17	km
e	$2.71 \cdot 10^{-4}$	
i	13.72	deg
Ω	12.21	deg
ω	317.51	deg
ν	227.82	deg
C_{RA}/m	0.015	m^2/kg

declination, δ) every 8 s. Gaussian noise with zero-mean and $\sigma_\alpha = \sigma_\delta = 1$ arcsec has been added to the simulated right ascension and declination measurements.

The problem was solved on the grid of maneuver epoch, t_M , and for each possible combination of the three tracks, i.e.: {1}, {2}, {3}, {1, 2}, {1, 3}, {2, 3} and {1, 2, 3}, following the method presented in Section 2, aimed at minimizing \sqrt{J} by the addition of a maneuver. Figures 7, 8 and 9 show $|\hat{u}|$ (red) and \sqrt{J} (purple) for the radial, in-track and cross-track maneuver cases, respectively, and three tracks (hat denotes estimated values). The red horizontal dashed line represents the true magnitude of the maneuver and the black vertical dashed line the true maneuver epoch. There are several local minima on $|\hat{u}|$ and \sqrt{J} that not always coincide, with a time separation of around 1 day, which is the orbital period. This non-linear behavior suggests that a joint estimation of both the maneuver epoch and magnitude may not be a good choice, at least for an initial maneuver estimation approach.

The details of each \sqrt{J} local minima are compiled in Table 2, where apart from the maneuver estimation results, the errors in the semi-major axis, eccentricity and inclination estimations (corresponding to the pre-maneuver orbit after the application of the estimated maneuver) are also shown. Firstly, in the case of the radial burn, the solution with lowest $|\hat{u}|$ does not exactly correspond to the true solution, although the three local minima differ in less than 0.2% with respect to the true magnitude. Besides, the one corresponding to the true solution has the lowest error in semi-major axis and eccentricity. Secondly, in the case of the in-track burn, there are two solutions on the vicinity of the epoch (one hour before and one hour after). They have the lowest $|\hat{u}|$, as well as lowest orbital differences. Thirdly, in the case of the cross-track burn, there are two solutions with lower $|\hat{u}|$ than the one of the true maneuver and the one corresponding to the true solution has the lowest orbital differences. Finally, in the case of the cross track burn of high magnitude, there are solutions with $\sqrt{J} > 1$, unlike in the rest of the cases, because of the high magnitude of the burn. This last case was included as a limiting one to study potential limitations of the linearization. As opposed to the cross-track burn of 1 m/s, the estimated

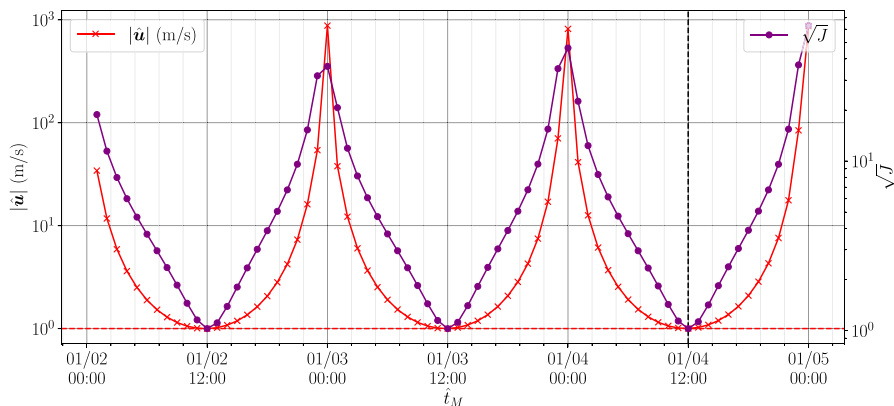


Fig. 7 Sat#0 scenario, T2O methodology, radial burn: $|\hat{u}|$ and \sqrt{J} distribution with maneuver time and tracks {1, 2, 3}

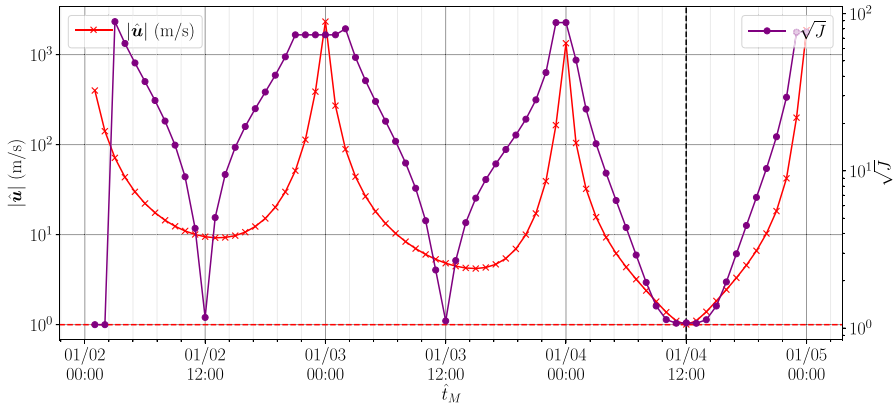


Fig. 8 Sat#0 scenario, T2O methodology, in-track burn: $|\hat{u}|$ and \sqrt{J} distribution with maneuver time for tracks {1, 2, 3}

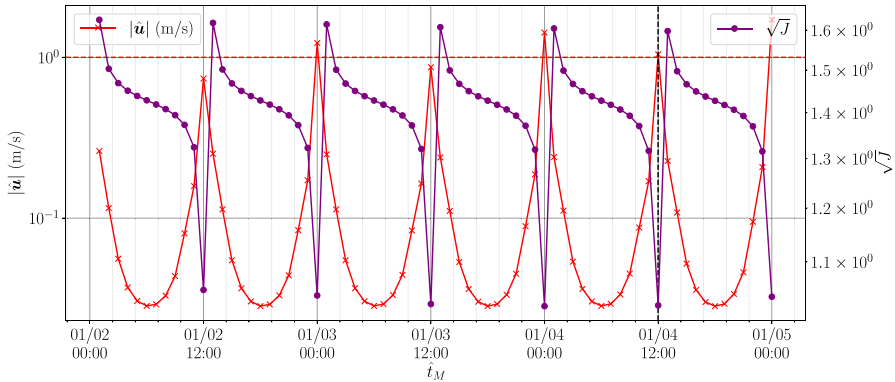


Fig. 9 Sat#0 scenario, T2O methodology, cross-track burn: $|\hat{u}|$ and \sqrt{J} distribution with maneuver time for tracks {1, 2, 3}

maneuver magnitude in the in-track direction is not negligible, thus making the error in the semi-major axis to increase. However, the solution with lowest \sqrt{J} corresponds to the true solution and the total estimated maneuver magnitude is of 9.95 m/s, i.e.: less than 0.5% error with respect to the true value.

It is expected that cases involving three tracks, {1, 2, 3}, are the best conditioned ones. Figure 10 shows the $|\hat{u}|$ and \sqrt{J} distribution of the \sqrt{J} local minima found for each combination of tracks, along the semi-major axis and eccentricity errors in the radial burn case. Although several \sqrt{J} local minima are found when considering only a single track, even with $|\hat{u}| \sim 1\text{m/s}$ and $\sqrt{J} \sim 1$, more information (tracks) is required to reliably estimate the effect of the maneuver on the orbit. Only when two and three tracks are involved, solutions with $|a - \hat{a}| < 10\text{m}$ and $|e - \hat{e}| < 10^{-5}$ are found and the local minima converge to the truth. In other words, although the methodology can be used with a single track, the lack of information in that case

Table 2 Sat#0 scenario, T2O methodology: Details of each \sqrt{J} local minima for association of tracks {1, 2, 3}

case	t_M	\sqrt{J}	\hat{u}_R (m/s)	\hat{u}_I (m/s)	\hat{u}_C (m/s)	$ \hat{\mathbf{u}} $ (m/s)	$ \hat{a} - a $ (km)	$ \hat{e} - e $	$ \hat{i} - i $ (deg)
Radial burn $u_R = 1\text{ m/s}$	01/02-12:00	1.0258	0.9964	0.0003	0.0339	0.9970	0.8617	7.88×10^{-6}	1.40×10^{-3}
	01/03-12:00	1.0250	0.9988	0.0002	0.0347	0.9994	0.3586	1.50×10^{-6}	6.09×10^{-4}
	01/04-12:00	1.0247	1.0012	0.0002	0.0349	1.0018	0.0045	1.05×10^{-6}	6.44×10^{-4}
In-track burn $u_I = 1\text{ m/s}$	01/02-12:00	1.1686	-9.4404	0.8948	-0.1174	9.4835	3.4345	1.99×10^{-3}	4.20×10^{-3}
	01/03-12:00	1.1105	-4.7165	0.9757	-0.0031	4.8163	0.9697	6.04×10^{-4}	1.31×10^{-3}
	01/04-11:00	1.0740	-0.4572	0.9991	0.0155	1.0988	0.0343	1.96×10^{-5}	1.33×10^{-4}
	01/04-13:00	1.0730	0.4697	0.9979	-0.0204	1.1031	0.2660	8.20×10^{-7}	2.57×10^{-4}
Cross-track burn $u_C = 1\text{ m/s}$	01/02-12:00	1.0511	0.0009	-0.0002	0.7383	0.7383	0.8719	1.27×10^{-5}	6.83×10^{-3}
	01/03-00:00	1.0418	-0.9289	-0.0006	-0.8035	1.2282	0.7575	1.97×10^{-4}	5.34×10^{-3}
	01/03-12:00	1.0275	0.0011	-0.0002	0.8681	0.8681	0.3685	4.38×10^{-6}	3.66×10^{-3}
	01/04-00:00	1.0239	-1.0640	-0.0007	-0.9505	1.4268	0.4169	2.57×10^{-4}	1.62×10^{-3}
	01/04-12:00	1.0253	0.0013	-0.0003	1.0428	1.0428	0.0050	2.06×10^{-6}	7.91×10^{-4}
Cross-track' burn $u_{C'} = 10\text{ m/s}$	01/02-12:00	3.2976	-0.0001	-0.0228	7.0493	7.0493	0.8511	1.20×10^{-5}	5.47×10^{-2}
	01/03-00:00	2.7915	0.5239	-0.0243	-7.5501	7.5683	0.8670	1.01×10^{-4}	3.25×10^{-1}
	01/03-12:00	2.1017	0.0001	-0.0268	8.2848	8.2848	0.8771	1.25×10^{-5}	3.17×10^{-2}
	01/04-00:00	1.5020	0.0451	-0.0290	-8.9648	8.9650	0.8848	3.52×10^{-6}	3.51×10^{-1}
	01/04-12:00	1.0220	0.0002	-0.0322	9.9515	9.9515	0.8906	1.30×10^{-5}	8.94×10^{-4}

may lead to an insufficiently accurate orbit estimation, potentially compromising subsequent cataloging activities. The methodology allows the linkage of pre-maneuver and post-maneuver tracks, thus reducing the number of tracks required after the maneuver if compared to a new detection from scratch (three or four tracks are usually required [4]) that considers only post-maneuver tracks.

4.1.2 Double burns, O2O methodology

The first assessment of the O2O methodology is aimed at performing a preliminary analysis of the method and comparison against Lambert’s problem solution. To do so, an initial state vector was propagated from t_0 up to $t_0 + 7$ days considering two impulsive burns in the local RIC frame. As in Section 4.1.1, this orbit will be referred to as *reference orbit* and six cases have been studied: 1) two radial burns (RR), 2) two in-track burns (II), 3) two cross-track burns (CC), 4) radial and in-track burns (RI), 5) radial and cross-track burns (RC) and 6) in-track and cross-track (IC) burns. The simulated burns are $\mathbf{u}_1 = +0.1 \mathbf{e}_i \text{ m/s}$ and $\mathbf{u}_2 = -0.1 \mathbf{e}_i \text{ m/s}$, being \mathbf{e}_i the

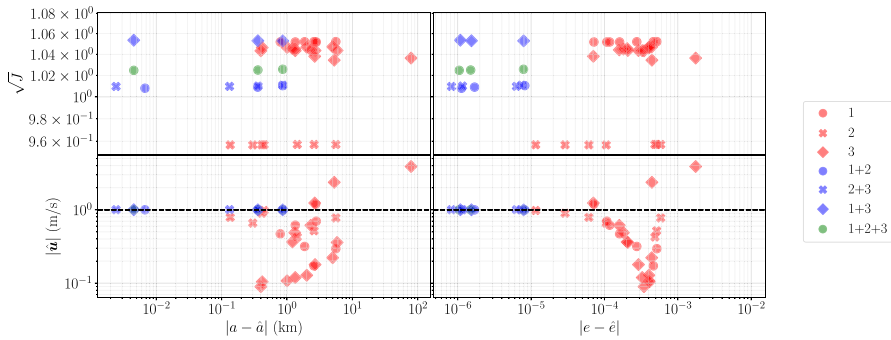


Fig. 10 Sat#0 scenario, T2O methodology, radial burn: $|u|$ and \sqrt{J} distribution of the \sqrt{J} local minima found for each track association

unitary vector in the R, I or C direction, i.e.: the sense of the first burn is positive, while the one of the second is negative with respect to the RIC frame. The burns are simulated at 12:00 of the 3rd and 4th days. As before, the pre-maneuver orbit was generated by performing the same propagation as the reference orbit but without considering the maneuvers. On the other hand, the post-maneuver orbit was generated by performing a back-propagation of the last state vector of the reference orbit without considering the maneuvers. The initial state vector is the same as in the T2O simulated scenario.

In this case, the outcome of the maneuver estimation method are the two estimated burns, \hat{u}_1 and \hat{u}_2 , for each \hat{t}_{M1} and \hat{t}_{M2} in the mesh used to sample \mathcal{T} . Figure 11 shows the distribution of the total velocity increase, i.e.: $|\hat{u}_1| + |\hat{u}_2|$, along $[\hat{t}_{M1}, \hat{t}_{M2}] \in \mathcal{T}$ in the *II* (left) and *RI* (right) cases. Note that solutions with $|\hat{u}| > 5$ m/s have been discarded. This representation, known as porkchop plot and typically used for interplanetary transfers, provides the velocity increase required for each combination of \hat{t}_{M1} and \hat{t}_{M2} that connects the pre-maneuver and post-maneuver orbits. Since there are no metrics to select a candidate estimation besides the maneuver magnitude, the optimal maneuver, i.e. minimum $|\hat{u}| = |\hat{u}_1| + |\hat{u}_2|$ is accepted as solution. However, in Fig. 11, the presence of multiple local minima confirms the existence of maneuvers with similar control effort that connect the two orbits. In principle, they are equivalent from the association point of view, meaning that an accurate estimation of the maneuver epoch is not ensured.

The three lowest $|\hat{u}|$ of each case are presented in Table 3. In most cases, the corresponding \hat{t}_{M1} and \hat{t}_{M2} do not match the true values and $|\hat{u}| < |u|$, meaning that a maneuver with lower $|u|$ than the true one has been found. The norm of the overdetermined linear system, ϵ , suggests that the linear system has been properly solved. As expected, those cases involving an in-track burn present higher values of ϵ (although within acceptable bounds), being this an indicator of the higher non-linearity in this direction.

In order to evaluate the accuracy of the estimations, the resulting maneuver magnitudes at t_{M1} and t_{M2} (true values) for each case are summarized in Table 4. As expected, the estimated values of the burns coincide with the true ones, even if

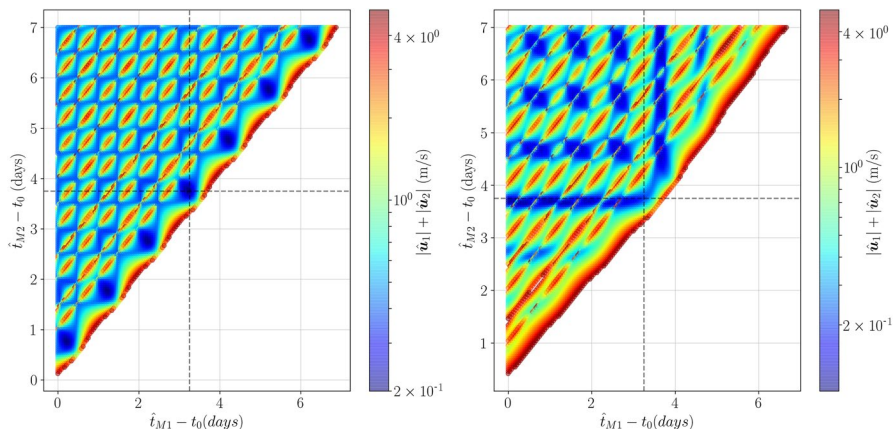


Fig. 11 Sat#0 scenario, O2O methodology, *II* (left) and *RI* (right): Porkchop plot

considered independently. This shows how the methodology is able to find a solution that matches the true maneuver, although it may not be selected as lower $|\mathbf{u}|$ ones are found. This is expected, since there are more variables driving operator’s maneuver plans, such as working hours, holidays or frequency, among others. Given the unavailability of this external data, sticking to lowest $|\mathbf{u}|$ solution is suggested, even though in some cases it may not correspond to the true one. In any case, both are expected to solve the linkage problem and as soon as more tracks after the maneuver are received, the maneuver estimation (not only magnitude on each direction but also time) could be refined.

4.2 Sat#1 scenario: real observations and SK maneuvers

Once the performance of the methodologies with simulated data has been assessed, a scenario with real observations is studied to confirm the adequacy of the proposed method. It consists in a real GEO satellite providing coverage to Europe and 4 telescopes from the ISON network. The tracks are distributed along two weeks and the impulsive burns performed by the RSO are: 1) $|\mathbf{u}_1| \sim 1.17$ m/s NS and 2) $|\mathbf{u}_2| \sim 20$ mm/s EW burn, separated around 62 h. The timeline of tracks and burns is shown in Fig. 12.

4.2.1 Single burns, T2T methodology

In order to understand the details of the T2O methodology performance, a subset of 9 tracks, depicted as red dotted lines in Fig. 12, from one of the telescopes has been used.

NS burn Five tracks, {1, 2, 3, 4, 5}, were available after the first burn and before the second burn and associations of two and three tracks have been considered for

Table 3 Sat#0 scenario, O2O methodology: Three solutions with lower $|\hat{u}|$ of each case

Case	\hat{t}_{M1}	\hat{t}_{M2}	ϵ	$ \hat{u}_1 $ (m/s)	$ \hat{u}_2 $ (m/s)	$ \hat{u} $ (m/s)
RR	01/01-00:00	01/01-17:00	1.54×10^{-15}	0.02249	0.14996	0.17245
	01/07-07:00	01/08-00:00	1.55×10^{-15}	0.14998	0.02248	0.17247
	01/01-12:00	01/02-05:00	1.50×10^{-15}	0.02229	0.15047	0.17276
II	01/04-06:00	01/04-18:00	1.75×10^{-13}	0.09997	0.09997	0.19994
	01/05-06:00	01/05-18:00	1.76×10^{-13}	0.10000	0.09999	0.19999
	01/03-06:00	01/03-18:00	1.74×10^{-13}	0.10001	0.10000	0.20001
CC	01/03-18:00	01/04-18:00	1.67×10^{-17}	0.05570	0.14426	0.19995
	01/02-18:00	01/04-18:00	4.42×10^{-17}	0.02785	0.17210	0.19996
	01/01-18:00	01/04-18:00	5.63×10^{-17}	0.01858	0.18138	0.19996
RI	01/03-12:00	01/07-23:00	6.41×10^{-08}	0.06567	0.03608	0.10175
	01/01-03:00	01/04-17:00	4.44×10^{-10}	0.00538	0.10803	0.11341
	01/01-04:00	01/04-17:00	6.17×10^{-10}	0.00723	0.10652	0.11376
RC	01/06-19:00	01/07-16:00	8.57×10^{-15}	0.08623	0.05103	0.13726
	01/05-19:00	01/06-16:00	8.58×10^{-15}	0.08811	0.04916	0.13727
	01/04-19:00	01/05-16:00	8.59×10^{-15}	0.08997	0.04731	0.13728
IC	01/02-21:00	01/04-06:00	5.89×10^{-11}	0.00087	0.14052	0.14139
	01/01-21:00	01/04-06:00	1.47×10^{-10}	0.00088	0.14067	0.14155
	01/04-06:00	01/06-20:00	9.74×10^{-11}	0.14042	0.00115	0.14158

Table 4 Sat#0 scenario, O2O methodology: Error in the estimation at t_{M1} and t_{M2}

case	ϵ	$ \hat{u}_1 - u_1 $ (m/s)	$ \hat{u}_2 - u_2 $ (m/s)	$ \hat{u} - u $ (m/s)
RR	3.05×10^{-15}	1.15×10^{-05}	1.15×10^{-05}	1.00×10^{-08}
II	1.75×10^{-13}	2.81×10^{-05}	2.81×10^{-05}	5.62×10^{-05}
CC	3.84×10^{-21}	3.00×10^{-08}	7.00×10^{-08}	4.00×10^{-08}
RI	6.87×10^{-14}	1.15×10^{-05}	2.81×10^{-05}	1.66×10^{-05}
RC	1.45×10^{-15}	1.15×10^{-05}	7.00×10^{-08}	1.16×10^{-05}
IC	6.24×10^{-14}	2.81×10^{-05}	7.00×10^{-08}	2.80×10^{-05}

the estimation of the maneuver. Figure 13 shows the distribution of \hat{u}_i and \sqrt{J} with \hat{t}_M , for the association of tracks {1, 3}. The horizontal dashed lines correspond to the reference values of each maneuver component, while the vertical dashed line

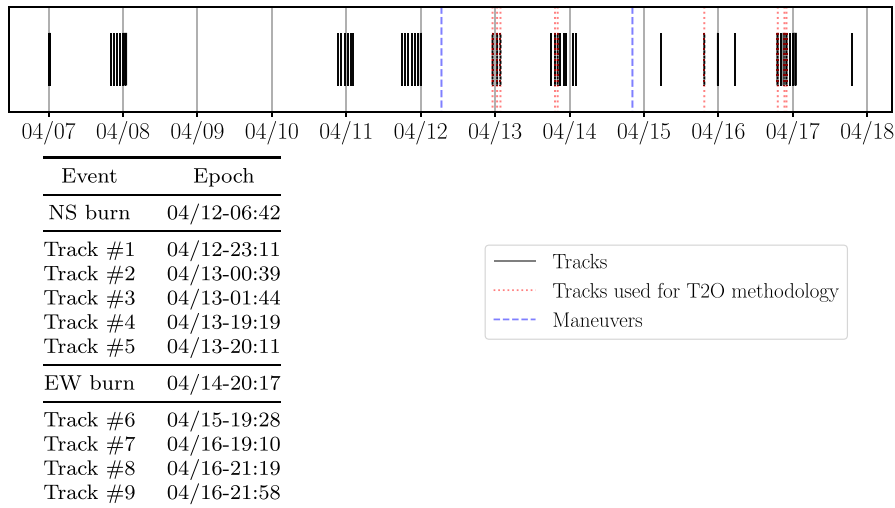


Fig. 12 Sat#1 scenario: Timeline of tracks and maneuvers (month/day) and details of the two burns and the subset of tracks used for the T2O methodology

represents the reference epoch of the maneuver. There is a local minima of \sqrt{J} that coincides with the reference epoch and at which \hat{u}_i values match the reference velocity increase values. However, there are two additional \sqrt{J} local minima half orbital period before and after the reference t_M . These correspond to different maneuvers that are compatible with the orbit and tracks considered and in fact they present similar $|\hat{u}|$ values.

The local minima corresponding to each solution with $|\hat{u}| < 2 \text{ m/s}$ are presented in Table 5. The estimations are consistent along the different track associations and

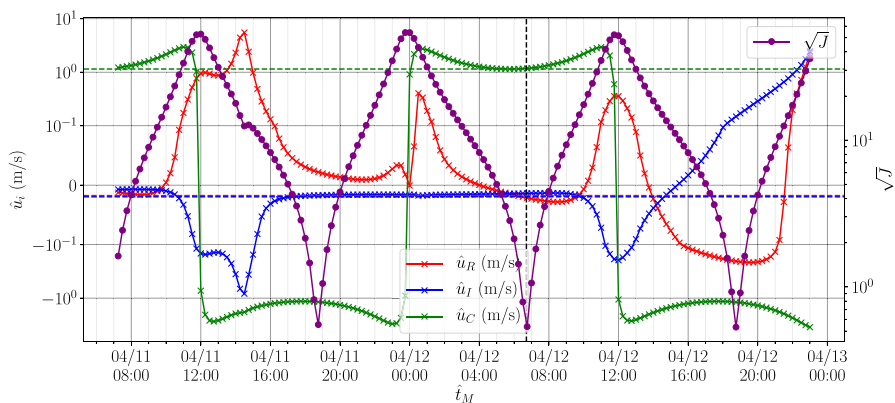


Fig. 13 Sat#1 scenario, T2O methodology, NS burn: \hat{u}_i and \sqrt{J} variation along \hat{t}_M for track association {1,3}

a solution close to the reference maneuver ($t_M = 12\text{-}06\text{:}42$ and $|\hat{\mathbf{u}}| \sim 1.17$ m/s) is found. Besides, $\sqrt{J} \sim 1$ indicated that the maneuver is estimated in such a way that the residuals of the observation matches the expected sensor noise. Note that associating three tracks allows to discard a pair of local minima with $\sqrt{J} \sim 3.6$, while this is not possible if only associations of two tracks are used. The solution with lowest $|\hat{\mathbf{u}}|$ from the associations of three tracks, that would be identified as the the maneuver in a hard-decision making environment, would be $|\hat{\mathbf{u}}| = 1.1512$ m/s at $\hat{t}_M = 12\text{-}18\text{:}30$ (from association $\{1, 3, 5\}$), i.e.: 1% of error in magnitude and around 12 h difference in epoch with respect to the reference value. This solution correspond to a burn with opposite sense in the cross-track direction performed on the opposite orbital point (around half period separation).

EW burn In this case, four tracks, $\{6, 7, 8, 9\}$, were available after the second burn and again, associations of up to three tracks have been considered for the estimation of the maneuver. Figure 14 shows the distribution of every $|\mathbf{u}|$ local minima found along $|\mathbf{u}|$ and \sqrt{J} . Even though the estimation of this burn is more challenging than the previous NS one due to the lower impulse involved, which is translated into a fainter maneuver footprint on the residuals, associations of two and three tracks are able to estimate a burn within the order of magnitude of the reference value. The estimation obtained with the association of three tracks and lowest $|\hat{\mathbf{u}}|$ is $|\hat{\mathbf{u}}| = 44$ mm/s and the corresponding maneuver epoch is estimated with less than one hour of error ($\hat{t}_M = 14\text{-}21\text{:}15$).

4.2.2 Double burns, O2O methodology

The pre-maneuver and post-maneuver orbits, estimated with real observations, have been used to study the performance of the O2O methodology. Figure 15 shows the resulting porkchop plot (zoomed in the vicinity of the reference solution and discarding solutions with $|\hat{\mathbf{u}}| > 5$ m/s) that, as in the simulated scenario, present many local minima corresponding to maneuvers able to link the two orbits.

Table 6 presents the four optimal solutions (i.e.: lowest $|\hat{\mathbf{u}}|$). Note that $|\hat{t}_{M1} - t_{M1}| < 15$ min and $|\hat{t}_{M2} - t_{M2}| < 2$ h in the case of the optimal solution. Although this maneuver is different than the reference one in terms of $|\hat{\mathbf{u}}_1|$ and $|\hat{\mathbf{u}}_2|$, if independently considered, the total velocity increase, $|\hat{\mathbf{u}} - \mathbf{u}|$ is estimated with an error lower than 1.5% of the reference value. This means that two potential burns whose $|\hat{\mathbf{u}}|$ is of the same order of magnitude of the real one can be estimated. Besides, Table 6 present the results obtained if Lambert's problem is solved in the same \hat{t}_{M1} and \hat{t}_{M2} grid than the methodology. The reason behind the unaccurate results provided by Lambert's problem is the orbit dynamics mismodelling of the Lambert's problem solution (two-body motion). This justifies the choice of the linearized orbit model including perturbations over a two-body motion model for a robust approach.

The total estimated maneuver magnitude at t_{M1} and t_{M2} (reference epochs) is $|\hat{\mathbf{u}}| = 1.29$ m/s, i.e., a relative error of less than 10%. Again, without additional information it is not possible to select this solution since the local minima have

Table 5 Sat#1 scenario, T2O methodology, NS burn: \sqrt{J} local minima found for each association of tracks

Tracks	\hat{t}_M	\sqrt{J}	$ \hat{u} $ (m/s)
{1, 2}	12-18:45:00	0.53	1.22
{1, 2}	11-18:45:00	0.54	1.18
{1, 2}	12-06:45:00	0.54	1.18
{1, 3}	12-18:45:00	0.53	1.21
{1, 3}	12-06:45:00	0.54	1.18
{1, 3}	11-18:45:00	0.55	1.18
{1, 4}	11-18:45:00	0.87	1.18
{1, 4}	12-06:45:00	0.87	1.18
{1, 4}	12-18:30:00	1.17	1.15
{1, 5}	11-18:45:00	0.79	1.18
{1, 5}	12-06:45:00	0.80	1.18
{1, 5}	12-18:30:00	1.08	1.15
{2, 3}	12-18:45	0.59	1.20
{2, 3}	11-18:45	0.60	1.18
{2, 3}	12-06:45	0.60	1.18
{2, 4}	11-18:45	1.15	1.18
{2, 4}	12-06:45	1.27	1.19
{2, 4}	12-18:30	1.29	1.15
{2, 5}	11-18:45	1.01	1.19
{2, 5}	12-06:45	1.12	1.19
{2, 5}	12-18:30	1.12	1.15
{3, 4}	11-18:45	1.18	1.19
{3, 4}	12-06:45	1.31	1.19
{3, 4}	12-18:30	1.40	1.15
{3, 5}	11-18:45	1.02	1.19
{3, 5}	12-06:45	1.11	1.20
{3, 5}	12-18:30	1.23	1.14
{4, 5}	11-18:45	0.76	1.23
{4, 5}	12-06:45	0.79	1.25
{4, 5}	13-06:30	0.78	1.11
{1, 3, 4}	11-18:45	1.03	1.18
{1, 3, 4}	12-06:45	1.05	1.18
{1, 3, 4}	12-18:30	3.64	1.15
{1, 3, 5}	11-18:45	0.92	1.18
{1, 3, 5}	12-06:45	0.95	1.18
{1, 3, 5}	12-18:30	3.63	1.15

similar values of $|\hat{u}|$ and are able to solve the linkage problem. A projection of this distribution on the $\hat{t}_{M2} - \hat{t}_{M1}$ plane (Fig. 16) illustrates this fact and also justifies the suitability of defining a threshold u_{max} such that $|\hat{u}| < u_{max}$ to reduce the number of solutions. In this case, there are a total of 96,141 solutions, which

Fig. 14 Sat#1 scenario, T2O methodology, EW burn: $|\mathbf{u}|$ and \sqrt{J} distribution of the \sqrt{J} local minima found for each combination of tracks

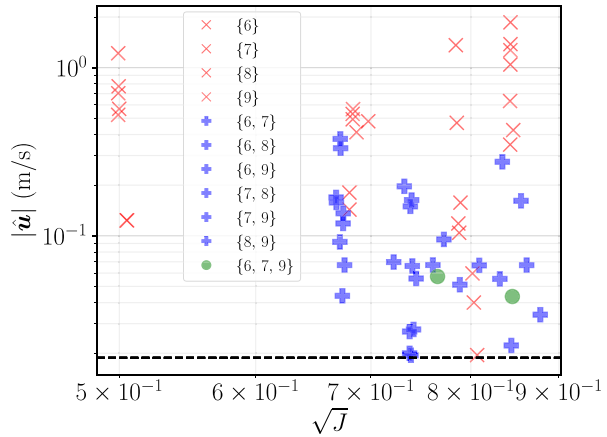
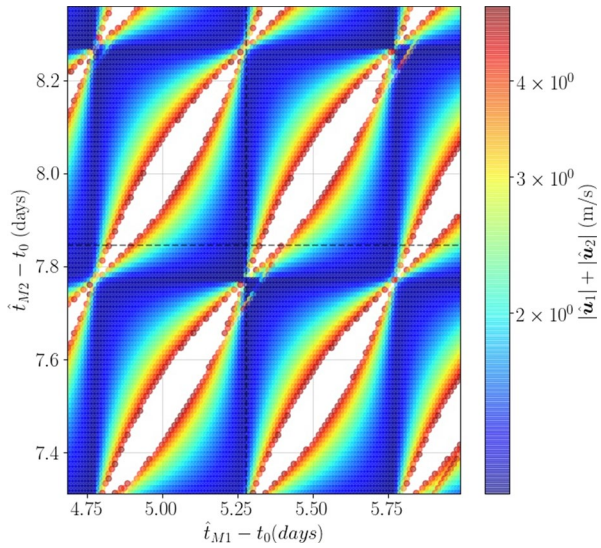


Fig. 15 Sat#1 scenario, O2O methodology: Porkchop plot (zoomed on the vicinity of the reference solution)



is reduced by 20% with $u_{max} = 5$ m/s and 54% with $u_{max} = 2$ m/s. Note this is very relevant for the association framework since it provides a mean to prune hypotheses, thereby reducing the computational load. Still, the computational burden associated to the maneuver detection and estimation methodology is not reduced, since these solutions have to be obtained first.

Table 6 Sat#1 scenario, O2O methodology: Reference, estimated values of the maneuver (global and additional local minima) and Lambert’s problem solution

	t_{M1}	t_{M2}	ϵ	$ \mathbf{u}_1 $ (m/s)	$ \mathbf{u}_2 $ (m/s)	$ \mathbf{u} $ (m/s)
Reference	04/12-06:42	04/14-20:17		1.1646	0.0199	1.1840
Estimated	04/12-06:30	04/14-18:30	3.36×10^{-10}	0.039	1.124	1.163
	04/13-06:30	04/13-18:45	1.65×10^{-12}	0.765	0.404	1.169
	04/12-18:30	04/15-06:30	1.72×10^{-10}	0.251	0.917	1.169
	04/12-06:30	04/14-18:45	1.26×10^{-10}	0.711	0.459	1.170
	04/12-18:15	04/15-06:30	1.25×10^{-10}	0.101	1.070	1.171
Lambert’s problem	04/11-12:00	04/15-18:30		0.043	0.577	0.619
	04/11-12:15	04/15-18:30		0.042	0.577	0.620
	04/11-11:45	04/15-18:30		0.044	0.576	0.620
	04/11-12:30	04/15-18:30		0.043	0.578	0.621

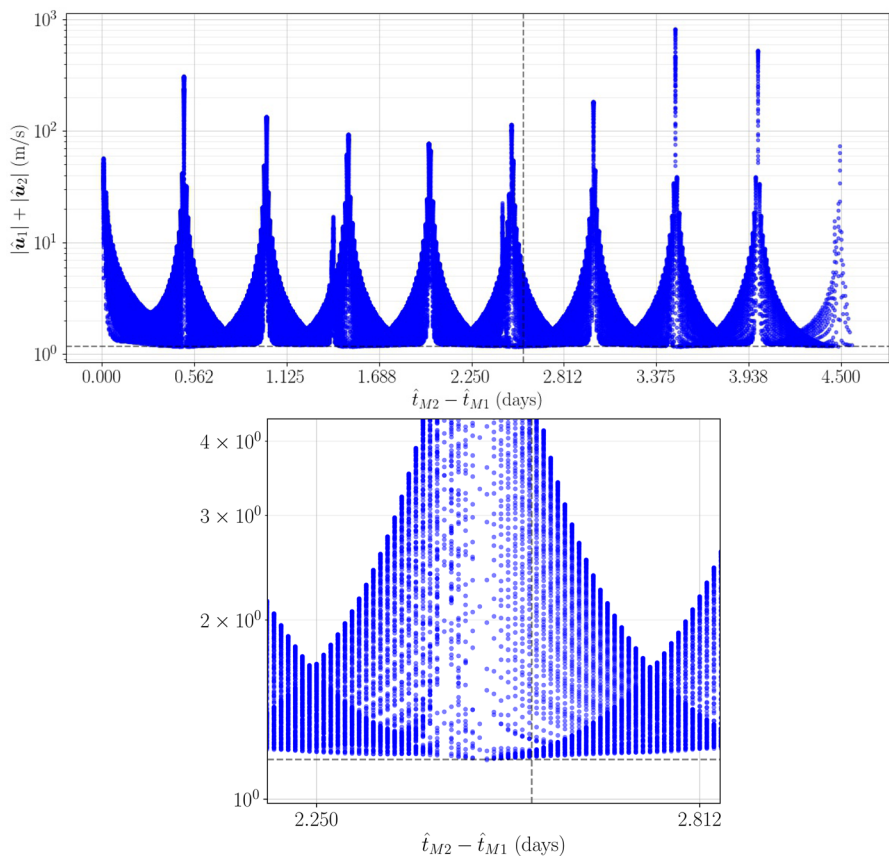


Fig. 16 Sat#1 scenario, O2O methodology: $|\hat{\mathbf{u}}_1| + |\hat{\mathbf{u}}_2|$ distribution along $\hat{t}_2 - \hat{t}_1$

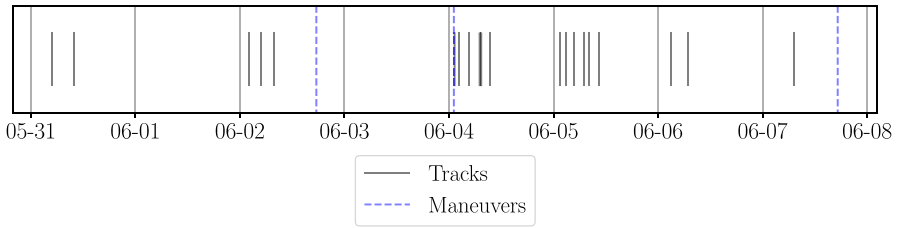
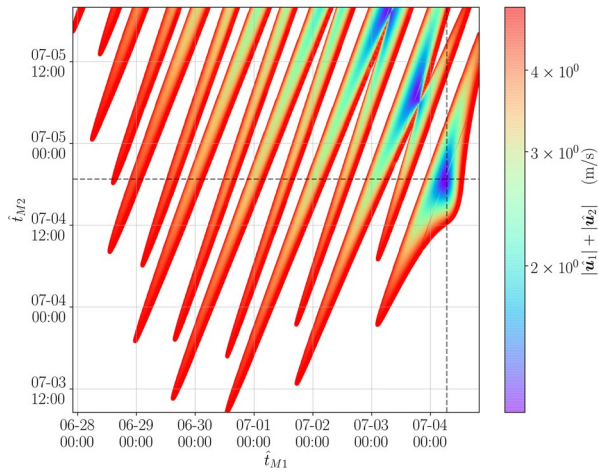


Fig. 17 Sat#2 scenario: Timeline of tracks and maneuvers (month/day)

Fig. 18 Sat#2 scenario, O2O methodology: Porkchop plot



4.3 Sat#2 scenario: real observations and SK maneuvers

This scenario focuses on a real GEO satellite and 9 telescopes from the ISON network. The tracks are distributed along one and a half weeks, as shown in Fig. 17, and the impulsive burns performed by the RSO are $|\mathbf{u}_1| \sim |\mathbf{u}_2| \sim 0.59$ m/s, in the in-track direction and separated 12 h. Since there are no observations between the two burns, only the O2O methodology has been applied. The pre-maneuver and post-maneuver orbits have been estimated by using all tracks before the first burn and after the second burn, respectively.

4.3.1 Double burns, O2O methodology

The porkchop plot, shown in Fig. 18, shows a clear $|\mathbf{u}|$ local minimum on the vicinity of the reference solution (dotted lines). Note that the shape of this porkchop plot is different than the one obtained for the double NS+EW burn (Section 4.2, Fig. 15) mainly because different directions are involved. There are less local minima and higher convexity in the current case, which, in principle, may lead to an easier identification of the solution that is closer to the reference solution.

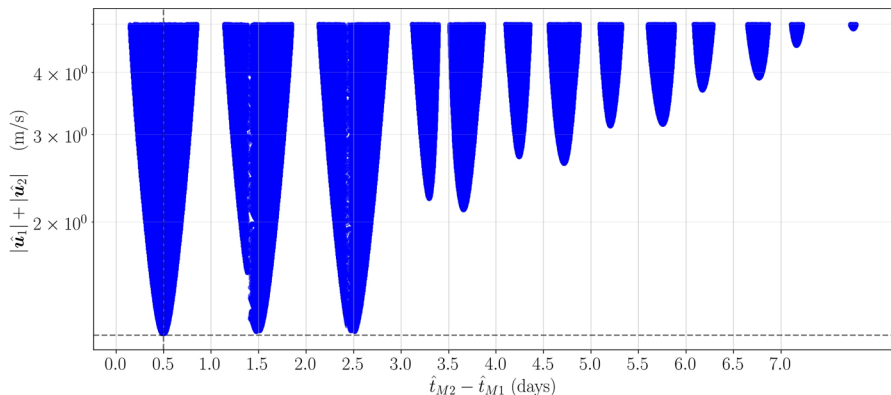


Fig. 19 $|u_1| + |u_2|$ distribution along $\hat{t}_2 - \hat{t}_1$ for Sat#2 scenario, O2O methodology

Table 7 Sat#2 scenario, O2O methodology: Reference, estimated values of the maneuvers (global and additional local minima) and Lambert’s problem solution (global and additional local minima)

	t_{M1}	t_{M2}	ϵ	$ u_1 $ (m/s)	$ u_2 $ (m/s)	$ u $ (m/s)
Reference	04-06:45	04-18:45		0.592	0.591	1.183
Estimated	04-06:26	04-18:45	4.95×10^{-10}	0.592	0.599	1.191
	03-19:26	05-06:51	2.11×10^{-8}	0.616	0.585	1.201
	03-07:38	05-19:57	4.18×10^{-6}	0.633	0.569	1.202
Lambert’s problem	04-07:14	04-17:45		0.637	0.701	1.338

Besides, the distribution of $|\hat{u}|$ along the time of flight, $\hat{t}_{M2} - \hat{t}_{M1}$, is presented in Fig. 19. There are three families of solutions centered at 0.5, 1.5 and 2.5 days (periodicity directly related to the orbital period) that correspond to the three regions around the three local minima in Fig. 18.

The estimated values of the solution with lowest $|\hat{u}|$ are presented in Table 7, along with the reference values. Both the burns independently (relative error of 0.08% and 1.46%) and the total impulse (relative error of 0.7%), as well as the epochs, can be properly determined. Apart from the global minima (first estimation presented), the two $|\hat{u}|$ local minima corresponding to the other two families of solutions have been included (second and third estimations presented) for completeness. They are feasible solutions with similar $|\hat{u}|$ but different \hat{t}_{M1} and \hat{t}_{M2} . Besides, Table 7 lists also the solution obtained using Lambert’s formulation, which exhibits a larger error when compared to the proposed method. In spite of the latter, this error is lower in relative terms than the one presented in Table 6 (Sat#1 scenario), since the dynamics mismodelling becomes more important as the time of flight increases (62 h in Sat#1 and 12 h in Sat#2).

4.4 Sat#3 scenario: real observations and large maneuvers

This scenario focuses on a real GEO satellite and 19 telescopes from the ISON network. The tracks are distributed along three days, as shown in Fig. 20 and the impulsive burns performed by the RSO are three in-track burns: $|\mathbf{u}_1| \sim 2.66$ m/s, $|\mathbf{u}_2| \sim 5.63$ m/s and $|\mathbf{u}_3| \sim 3.08$ m/s, separated around 12 h each.

4.4.1 Single burns, T2O methodology

As opposed to Section 4.2 (Sat#1), where the focus was on subsets of tracks, now we have considered every available track and study the distribution of the estimated maneuvers for each association of 1, 2, 3 and 4 tracks. Figure 21 shows the distribution of the track associations along the estimated maneuver magnitude error, $|\hat{\mathbf{u}}|$, and the estimated maneuver epoch error, $|t_M - \hat{t}_M|$. Besides, the vertical dashed black line represents the reference epoch of each burn. There is a clear benefit of increasing the number of associated tracks in terms of both epoch and magnitude estimation error. This is expected as more associated tracks imply more observations that are taken into account in the estimation process. Figure 22 presents the histograms of these errors for the particular case of the 3rd burn. There is a clear improvement in terms of the estimated epoch and magnitude error when moving from one or two tracks to three or four. Note that the O2O methodology could be used when dealing with associations of four tracks since in this case a reliable post-maneuver orbit can be usually obtained. However, the T2O methodology provides not only the estimation of the maneuver (magnitude, direction and epoch) but also \sqrt{J} , which can be used to prune solutions, of interest for the association problem.

For each of the three burns, the estimation obtained from associations of 3 and 4 tracks leading to the minimum maneuver magnitude has been selected and compared against the reference one in Table 8. The maneuver magnitude relative error (selected assoc.) is around 0.6% for the first burn, 1% for the second burn and 19% for the third burn. They are good results taking into account the relatively short time interval of observations considered for the estimation of the pre-maneuver orbit, as well as the short time between the maneuver and the post-maneuver tracks, just a few hours. In this regard, we may assume that, as long as the linearization of the dynamics is valid, the greater the time between the maneuver and the post-maneuver tracks the better, because of the time needed by the dynamics to make noticeable the maneuver effect. Besides, Table 8 includes an additional estimation obtained by considering every available track (a total of 27, 31 and 16 for the first, second and third burns, respectively).

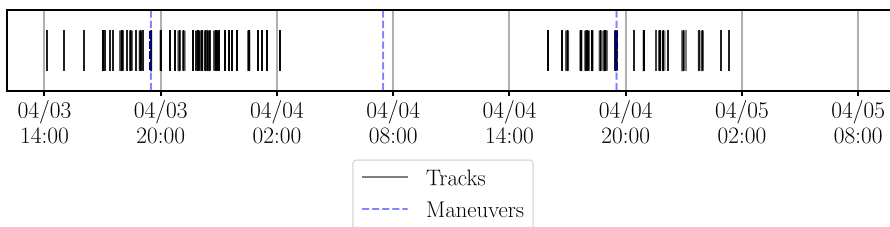


Fig. 20 Sat#3 scenario: Timeline of the tracks and burns (month/day)

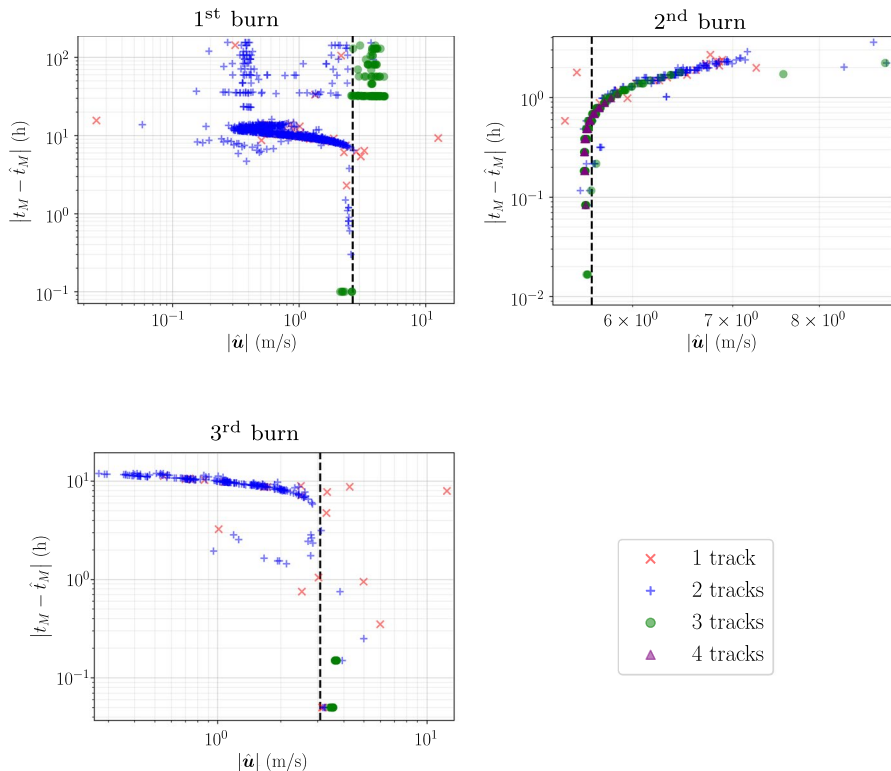


Fig. 21 Sat#3 scenario, T2O methodology: Distribution of the estimated maneuver magnitude and epoch error of each track association for the 1st, 2nd and 3rd burns

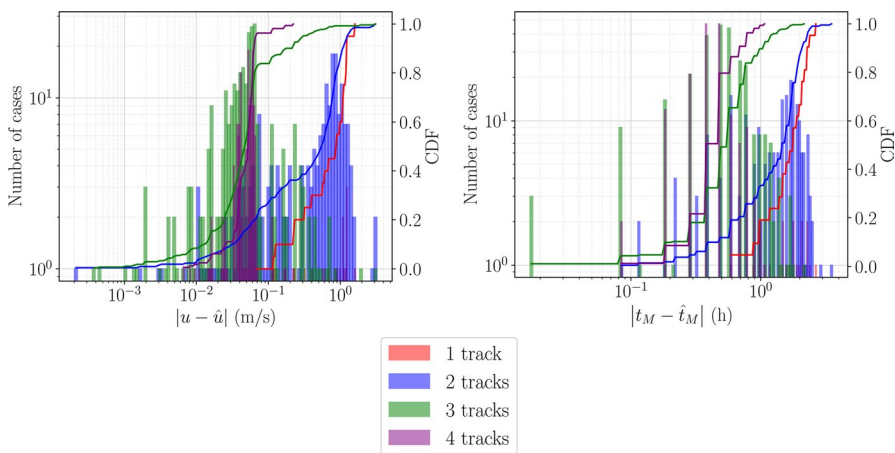


Fig. 22 Sat#3 scenario, T2O methodology, 3rd burn: Histogram of the estimated maneuver magnitude error (left) and epoch error (right)

Table 8 Sat#3 scenario, T2O methodology: Reference and estimated maneuvers

		t_M	$ \mathbf{u} $ (m/s)
1st burn	Reference	04/03-19:30	2.6609
	Estimated (selected assoc.)	04/03-19:30	2.6772
	Estimated (all tracks)	04/03-19:30	2.6756
2nd burn	Reference	04/04-07:29	5.6324
	Estimated (selected assoc.)	04/04-07:18	5.5710
	Estimated (all tracks)	04/04-07:00	5.5973
3rd burn	Reference	04/04-19:32	3.0817
	Estimated (selected assoc.)	04/04-19:41	3.6540
	Estimated (all tracks)	04/04-19:41	3.6518

Apart from the expected improvement of the maneuver magnitude estimation, the main benefit of considering more tracks is to discard $|\hat{\mathbf{u}}|$ local minima that, although similar, do not correspond to the true solution (as discussed in Section 4.2.1).

4.4.2 Double burns, O2O methodology

The O2O methodology has been applied to the same three burns but aimed at estimating two double burns: 1) 1st + 2nd burns and 2) 2nd + 3rd burns. To do so, the corresponding pre-maneuver and post-maneuver orbits have been estimated from the available observations.

The two resulting porkchop plots are shown in Fig. 23, including the reference epochs as black dashed lines. In both cases there is a clear $|\hat{\mathbf{u}}|$ global minima region and, opposed to the previous scenarios, there are no additional regions with local minima, mainly due to the relatively short domain of search, limited by the maneuvers timeline. Although the global minima of the first case (1st and 2nd burns, left) does not perfectly match the reference epochs, t_{M1} and t_{M2} , note that there is a delay of ~ 2 h between the estimated and reference maneuvers.

Moreover, the $|\hat{\mathbf{u}}|$ global minima are listed in Table 9. As in other scenarios, the error of the estimated maneuver magnitude of the burns, if considered independently (26% and 4% relative error for the first case, 35% and 106% for the second) is higher than the total impulse (11% for the first case, 15% for the second). These results confirm that the O2O methodology is able to deal with high impulses for GEO regime, confirming the validity of the linearization under high perturbations.

4.5 Sat#4 scenario: real observations and electric propulsion

This scenario focuses on a real GEO satellite with electric propulsion and 12 telescopes from the ISON network. As opposed to the previous satellites, equipped with chemical propulsion, this one performs continuous maneuvers with a low thrust electric propulsion. The tracks are distributed along several days, as shown

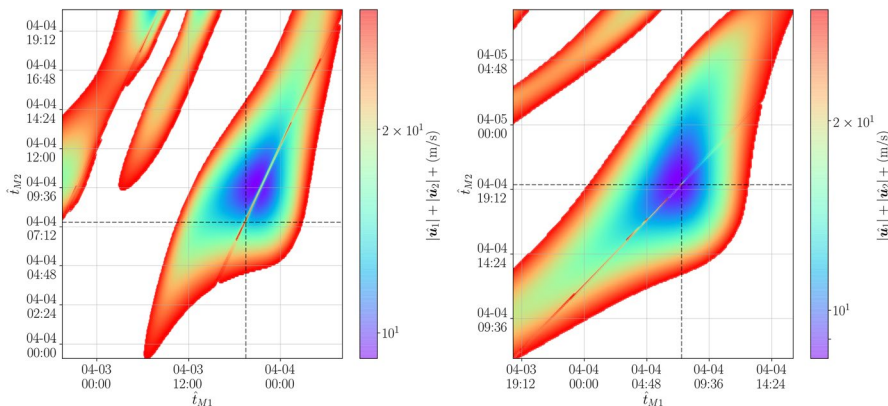


Fig. 23 Sat#3 scenario, O2O methodology: Porkchop plot: 1st and 2nd burns (left), 2nd and 3rd burns (right)

Table 9 Sat#3 scenario, O2O methodology: Reference and estimated values of the maneuvers for 1st and 2nd burn case, and 2nd and 3rd burns case

Burn		t_M	$ u $ (m/s)
1 st	Reference	03-19:31	2.6609
	Estimated	03-21:00	3.3439
2 nd	Reference	04-07:29	5.6324
	Estimated	04-09:49	5.8335
Total (1st + 2nd)	Reference		8.2933
	Estimated		9.1774
2 nd	Reference	04-07:29	5.6324
	Estimated	03-22:00	3.6750
3 rd	Reference	04-19:32	3.0817
	Estimated	04-09:07	6.3511
Total (2nd + 3rd)	Reference		8.7141
	Estimated		10.026

in Fig. 24 and the continuous burns performed by the RSO are: 1) $|u_1| \sim 48$ mm/s with a duration of 1.65 min and 2) $|u_2| \sim 135$ mm/s with a duration of 1.75 h, separated around 23 h (from start of the second to end of the first).

4.5.1 Single burns, T2O methodology

The T2O was applied to the estimation of the two burns, independently. Figure 25 shows the distribution of $|\hat{u}|$ and \sqrt{J} along \hat{t}_M for one of the associations of 4 tracks. Even though the burns are continuous, the method is able to locate local minima on \sqrt{J} assuming impulsive ones.



Fig. 24 Timeline of the Sat#4 scenario (month/day)

The selected solutions for each case (\sqrt{J} local minima with lowest $|\hat{u}|$) are listed in Table 10, where the reference values and the estimation using all tracks are included. Note that there are only 4 available tracks for the 2nd burn estimation and thus, the selected association contains all tracks. The first burn estimated magnitude relative error is around 29% (22% if considering all tracks) and the estimated epoch differs less than 3 h from the reference. However, the error in the second burn is much higher than the first (around 1400% in magnitude and around 2 h). Note that Table 10 (right) shows data from 04–20:00 for completeness, although the last observation used for the pre-maneuver orbit estimation is on 05–00:50, i.e.: solutions before this epoch should not be considered.

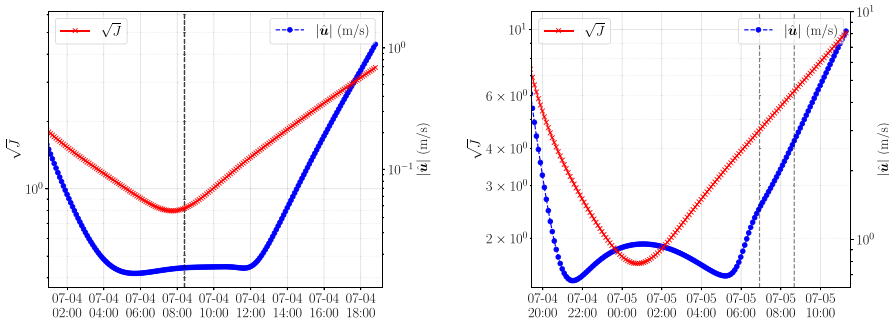


Fig. 25 Sat#4 scenario, T2O methodology: $|\hat{u}|$ and \sqrt{J} distribution with maneuver time for selected cases of the 1st burn (left) and 2nd burn (right)

Table 10 Sat#4 scenario, T2O methodology: Reference and estimated values of the maneuvers

		t_M	\sqrt{J}	$ \mathbf{u} $ (m/s)
1st burn	Reference	07/04-08:23 - 07/04-08:25		0.0479
	Estimated (selected assoc.)	07/04-05:42	0.42	0.0619
	Estimated (all tracks)	07/04-05:48	2.43	0.0584
2nd burn	Reference	07/05-06:56 – 07/05-08:41		0.1349
	Estimated (selected assoc.)	07/05-05:11	6.39	2.0207
	Estimated (all tracks)			

The main difference between the two burns is the duration: 1.65 min and 1.75 h, respectively and according to the reference. The first burn duration is so short that it can be assumed impulsive, while this does not hold for the second burn. On the other hand, the characterization of the second burn is not as accurate as the first one. Despite of this, the association of the pre-maneuver orbit and the post-maneuver tracks, is, in principle possible, since a compatible maneuver has been found with a reasonable matching between the pre-maneuver orbit and the post-maneuver tracks ($\sqrt{J} \sim 1$).

4.5.2 Double burns, O2O methodology

The double burn maneuver has been estimated with the O2O methodology, obtaining the porkchop plot presented in Fig. 26, where the two burns start and end epochs are depicted with black dashed lines. There are several local minima on the vicinity of the two reference impulsive burns.

Table 11 lists the reference and estimated values (global minima) of the two burns. The first and second burn estimated epoch error is of less than 1 h and 9 h, respectively, while the estimated total magnitude relative error is of 40%. Since the two maneuvers are jointly estimated, there is not a significant difference between the two estimated impulsive burns, i.e.: the epoch of the first is estimated with lower error, while the magnitude of the second is estimated more accurately. At this point, it is important to recall that the O2O methodology is intended to estimate the double burn impulsive maneuver that best approximates the real maneuver, which in this case is not a double burn impulsive maneuver. Therefore, this is an interesting test case with which the limitations of the methodology can be analyzed. In this case, the epochs and magnitude of the two separated burns are presented in Table 11 for completeness, but what is more relevant is the total magnitude (last two rows), which is estimated as 0.2572 m/s. The reference value is 0.1828 m/s, meaning that the obtained maneuver is of the same order of magnitude (around 40% of relative

Fig. 26 Sat#4 scenario, O2O methodology: Porkchop plot

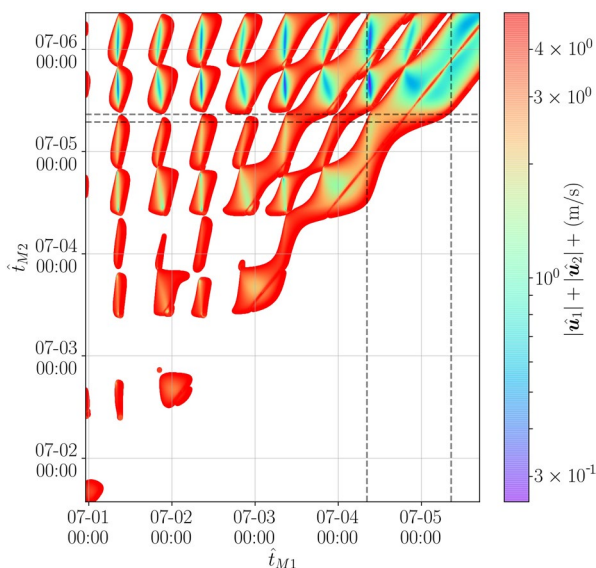


Table 11 Sat#4 scenario, O2O methodology: Reference and estimated values of the maneuvers

Burn		t_M	$ u $ (m/s)
1 st	Reference	07/04-08:23 - 07/04-08:25	0.0479
	Estimated	07/04-09:46	0.1355
2 nd	Reference	07/05-06:56 - 07/05-08:41	0.1349
	Estimated	07/05-16:08	0.1217
Total	Reference		0.1828
	Estimated		0.2572

error with respect to the reference value). Consequently, the association of the pre-maneuver and post-maneuver orbits is still possible given a suitable association framework.

5 Conclusions

Two novel methodologies for the detection and estimation of impulsive maneuvers have been presented. The first, focuses on track-to-orbit associations and is intended to detect and estimate single burn maneuvers, by determining the maneuver that applied to the pre-maneuver orbit minimizes the post-maneuver observations residuals. The second, conceived for the orbit-to-orbit association problem, approximates maneuvers of two burns as linear perturbations over the nominal ballistic motion of the RSOs. They do not require a-priori information nor fine tuning and are able to provide a first estimation of the maneuver that can be improved as more post-maneuver tracks are available. Besides, the two methodologies can be directly applied to observations from other sensors, such as radar or passive ranging stations.

Results show a good performance even when dealing with few tracks over relatively short time periods, including low impulses (~ 10 mm/s) and high impulses (~ 10 m/s) in GEO. Therefore, the authors propose the use of these methods in operational cataloging chains to increase the flexibility and robustness of the maintenance of the catalogs of RSOs. The computational time, compiled in Table 14 indicate that their integration would not harm the computation load of the association framework. As expected, there is a strong dependency on the size and step of the maneuver time grid considered to estimate the maneuver. Even though this grid was not optimized for reducing the computational burden, the computation time is of the order of seconds for a single maneuver detection and estimation with the T2O methodology and tens of seconds for the O2O methodology.

Moreover, the methods could be easily integrated in association frameworks, such as [5], for the evaluation of hypotheses involving tracks and orbits with maneuvers. Only by doing so, the T2O and O2O association problems under the presence of maneuvers could be solved. The rationale behind this, illustrated in the results, is that a single track is not enough for the T2O methodology to reliably estimate a

maneuver and thus, tracks must be associated before applying the T2O methodology. The detection and estimation of the maneuvers is performed using optimal control and simplified dynamical models, allowing to retain local minima for the solutions corresponding to different control efforts. In the case of a MHT framework, multiple local minima may translate into the expansion of the association tree, i.e.: generation of new hypotheses related to the maneuver, whereas in a hard-decision framework, this can be reduced to the optimal maneuver. In order to trim the association tree, or avoid taking a wrong decision, a maximum control effort can be defined such that $|\hat{u}| < u_{max}$. The value of u_{max} determines the number of hypotheses that may arise from a maneuver event and also avoid considering unrealistic maneuvers.

These methods have been conceived for the association problem, and therefore, their ultimate goal is not to provide the most accurate or realistic maneuver characterization, but one that allows the linkage between tracks and orbits (T2O) and orbits among themselves (O2O), particularly in data-scarce scenarios. Satellite operators may not always perform optimal maneuvers due to experience, safety or even working-hours scheme aspects and therefore optimal control metrics should not be blindly trusted. At the end, during cataloging operations the final goal is to ensure traceability between tracks and orbits so as to optimize SST network sensing data usage and detection of maneuvers, as well as to avoid duplicated objects. To reach this final goal, the two proposed methodologies should be integrated in an association framework. The authors are currently working on this integration and its application to real scenarios, which will provide end-to-end performance metrics, such as association metrics (true positives, false positives and false negatives) and total computational cost.

Appendix: Additional figures and tables

Table 12 Real satellites used in Section 4

Scenario	<i>a</i> (km)	<i>e</i>	<i>i</i> (deg)
Sat#1	42165.0	3.5×10^4	0.1
Sat#2	42163.9	3.1×10^5	4.2
Sat#3	42164.0	1.3×10^4	10.6
Sat#4	42164.7	9.7×10^5	0.0

Fig. 27 Distribution of the track duration of the real tracks used in Sat#1, Sat#2, Sat#3 and Sat#4 scenarios

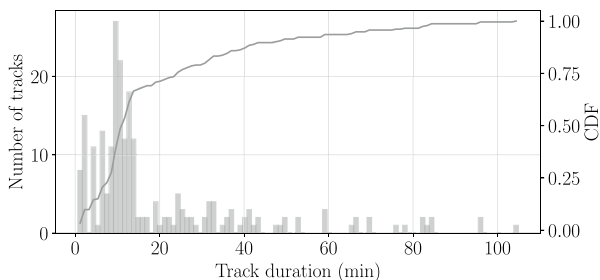


Fig. 28 Distribution of the observation spacing of the real tracks used in Sat#1, Sat#2, Sat#3 and Sat#4 scenarios

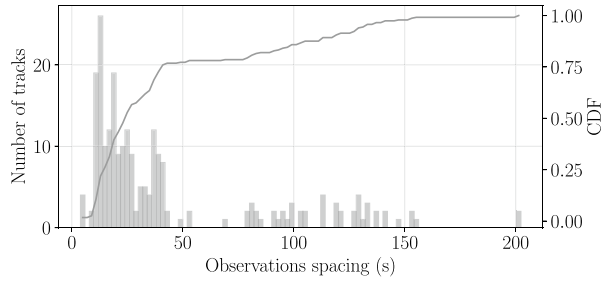


Table 13 Location of the telescopes from ISON used in Section 4

Telescope ID	Latitude (deg)	Longitude (deg)	Scenarios involved
10031	44.73	44.73	Sat#2, Sat#3, Sat#4
10059	39.14	39.14	Sat#4
10072	-21.60	-21.60	Sat#2
10088	53.35	53.35	Sat#3
10090	46.40	46.40	Sat#1, Sat#2, Sat#4
10092	48.56	48.56	Sat#3
10093	43.74	43.74	Sat#3
10094	43.74	43.74	Sat#3
10111	43.27	43.27	Sat#3
10114	49.64	49.64	Sat#2, Sat#4
10116	46.40	46.40	Sat#3
10149	45.02	45.02	Sat#3
10292	48.56	48.56	Sat#2, Sat#3, Sat#4
10301	40.35	40.35	Sat#3
10302	40.35	40.35	Sat#3
10313	43.74	43.74	Sat#3
10400	50.17	50.17	Sat#4
10401	50.17	50.17	Sat#4
10509	41.75	41.75	Sat#2, Sat#3, Sat#4
10536	44.72	44.72	Sat#2, Sat#3, Sat#4
10902	50.00	50.00	Sat#3, Sat#4
10905	50.00	50.00	Sat#3
10962	46.83	46.83	Sat#3
10963	46.83	46.83	Sat#2, Sat#4
10964	46.83	46.83	Sat#2, Sat#3, Sat#4
10982	43.74	42.65	Sat#3

Table 14 Computational time of the cases presented in Section 4

Scenario	Case	Time (s)	Comment
Sat#0	R	7.0	
	I	10.4	
	C	4.9	
	C'	9.4	
	RR	30.7	O2O methodology
	II	14.5	O2O methodology
	CC	10.8	O2O methodology
	RI	7.6	O2O methodology
	RC	7.4	O2O methodology
	IC	17.7	O2O methodology
Sat#1	1	4.7	average (17 association)
	2	5.3	average (11 association)
	1+2	79.5	O2O methodology
Sat#2	1+2	82.4	O2O methodology
Sat#3	1	54.2	average (1487 associations)
	1A	377.5	all tracks (27)
	2	3.0	average (665 association)
	2A	31.2	all tracks (21)
	3	2.2	average (577 associations)
	3A	17.3	all tracks (16)
	1+2	21.1	O2O methodology
	2+3	27.0	O2O methodology
Sat#4	1	5.2	average (186 associations)
	1A	19.1	all tracks (13)
	2	1.4	average (15 associations)
	2A	3.3	all tracks (4)
	3	1.7	average (309 associations)
	3A	5.7	all tracks (10)
	1+2	94.9	O2O methodology
	2+3	13.4	O2O methodology

Acknowledgements This project has received funding from the “Comunidad de Madrid” under the “Ayudas destinadas a la realización de doctorados industriales” program (project IND2017/TIC7700).

Funding Open Access funding provided thanks to the CRUE-CSIC agreement with Springer Nature.

Data availability The data underlying this article will be shared on reasonable request to the corresponding author.

Code availability The code developed and used for the preparation of this manuscript is commercial software property of GMV.

Declarations

Conflicts of interest The authors declare that they have no known competing financial interests or personal relationships that could have appeared to influence the work reported in this paper.

Open Access This article is licensed under a Creative Commons Attribution 4.0 International License, which permits use, sharing, adaptation, distribution and reproduction in any medium or format, as long as you give appropriate credit to the original author(s) and the source, provide a link to the Creative Commons licence, and indicate if changes were made. The images or other third party material in this article are included in the article's Creative Commons licence, unless indicated otherwise in a credit line to the material. If material is not included in the article's Creative Commons licence and your intended use is not permitted by statutory regulation or exceeds the permitted use, you will need to obtain permission directly from the copyright holder. To view a copy of this licence, visit <http://creativecommons.org/licenses/by/4.0/>.

References

1. Johnston, E.: Satellite signals, list of satellites in geostationary orbit. <http://www.satsig.net/sslist.htm> (2021)
2. Lafleur, C.: Spacecraft encyclopedia, a comprehensive census of all spacecraft ever launched. <http://claudelafleur.qc.ca/Spacecrafts-index.html> (2021)
3. Johnson, N.L., Stansbery, E., Whitlock, D.O., Abercromby, K.J., Shoots, D.: History of on-orbit satellite fragmentations. Tech. Rep. NASA orbital debris program office (2008)
4. Hill, K.: Maneuver detection and estimation with optical tracklets. In: Advanced Maui Optical and Space Surveillance Technologies Conference (2014)
5. Pastor, A., Escobar, D., Sanjurjo-Rivo, M., Águeda, A.: Object detection methods for optical survey measurements. In: 20th Advanced Maui Optical and Space Surveillance Technologies (2019)
6. Hill, K., Sabol, C., Alfriend, K.T.: Comparison of covariance based track association approaches using simulated radar data. *J. Astronaut. Sci.* **59**, 281–300 (2012)
7. Pulford, G.: Taxonomy of multiple target tracking methods. *IEE Proc. Radar Sonar Navig.* **152**(5), 291–304 (2005)
8. Stauch, J., Bessell, T., Rutten, M., Baldwin, J., Jah, M., Hill, K.: Joint probabilistic data association and smoothing applied to multiple space object tracking. *J. Guid. Control Dyn.* **41**(1), 19–33 (2018)
9. Bar-Shalom, Y., Daum, F., Huang, J.: The probabilistic data association filter. *IEEE Control Syst. Mag.* **29**, 82–100 (2010)
10. Milani, A., Gronchi, G.F., De' Michieli Vitturi, M., Knezevic, Z.: Orbit determination with very short arcs. I. Admissible regions. *Celest. Mech. Dyn. Astron.* **90**, 57–85 (2004)
11. Pirovano, L., Santeramo, D., Armellini, R., Di Lizia, P., Wittig, A.: Probabilistic data association: the orbit set. *Celest. Mech. Dyn. Astron.* **132**, 15 (2020)
12. Aristoff, J., Horwood, J., Singh, N., Poore, A., Sheaff, C., Jah, M.: Multiple hypothesis tracking (MHT) for space surveillance: Theoretical framework. *Adv. Astronaut. Sci.* **150**, 55–74 (2014)
13. Jones, B.A., Vo, B.-N.: A labeled multi-Bernoulli filter for space object tracking. In: Proc. AAS/AIAA spaceflight mech. meeting, pp. 11–15 (2014)
14. Siminski, J., Montenbruck, O., Fiedler, H., Schildknecht, T.: Short-arc tracklet association for geostationary objects. *Adv. Space Res.* **53**(8), 1184–1194 (2014)
15. Furfaro, R., Linares, R., Gaylor, D., Jah, M., Walls, R.: Resident space object characterization and behavior understanding via machine learning and ontology-based bayesian networks. In: Advanced Maui Optical and Space Surveillance Technologies Conference, p. 35 (2016)
16. Kelec, T., Hall, D., Hamada, K.: Satellite maneuver detection using two-line element (TLE) data. In: Advanced Maui Optical and Space Surveillance Technologies (AMOS) Conference (2007)
17. Lemmens, S., Krag, H.: Two-line-elements-based maneuver detection methods for satellites in low earth orbit. *J. Guid. Control Dyn.* **37**, 860–868 (2014)

18. Siminski, J., Fiedler, H., Flohrer, T.: Correlation of observations and orbit recovery considering maneuvers. In: AAS/AIAA Space Flight Mechanics (2017)
19. Shabarekh, C., Kent-Bryant, J., Keselman, G., Mitidis, A.: A novel method for satellite maneuver prediction. In: Advanced Maui Optical and Space Surveillance Technologies Conference, p. 11 (2016)
20. Holzinger M., Scheeres, D.: Object correlation and maneuver detection using optimal control performance metrics. In: Advanced Maui Optical and Space Surveillance Technologies (AMOS) Conference, p. E26 (2010)
21. Holzinger, M.J., Scheeres, D.J., Alfriend, K.T.: Object correlation, maneuver detection, and characterization using control distance metrics. *J. Guid. Control Dyn.* **35**, 1312–1325 (2012)
22. Mahalanobis, P.C.: On the generalised distance in statistics. *Proc. Nat. Inst. Sci. India* **2**, 49–55 (1936)
23. Luby, D.: Maneuver detection and reconstruction in data sparse systems with an optimal control based estimator. PhD thesis, University of Colorado Boulder (2015)
24. Huang, J., Hu, W., Xin, Q., Du, X.: An object correlation and maneuver detection approach for space surveillance. *Res. Astron. Astrophys.* **12**, 1402–1416 (2012)
25. Huang, J., Hu, W., Zhang, L.: Maneuver detection of space object for space surveillance. In: 6th European Conference on Space Debris (2013)
26. Yang, Z., Luo, Y., Zhang, J.: Nonlinear semi-analytical uncertainty propagation of trajectory under impulsive maneuvers. *Astrodynamics* **3**, 61–77 (2019)
27. Goff, G.M.: Orbit estimation of non-cooperative maneuvering spacecraft. PhD thesis, Department of the Air Force, Air University (2015)
28. Chernick, M., D’Amico, S.: New closed-form solutions for optimal impulsive control of spacecraft relative motion. *J. Guid. Control Dyn.* **41**, 301–319 (2018)
29. Ko, H.C., Scheeres, D.J.: Maneuver detection with event representation using thrust Fourier coefficients. *J. Guid. Control Dyn.* **39**, 1080–1091 (2016)
30. Montenbruck, O., Gill, E.: *Satellite Orbits: Models. Methods and Applications.* Springer, Berlin (2000)

Publisher’s note Springer Nature remains neutral with regard to jurisdictional claims in published maps and institutional affiliations.

Authors and Affiliations

Alejandro Pastor^{1,2}  · Guillermo Escibano² · Manuel Sanjurjo-Rivo² · Diego Escobar¹

✉ Alejandro Pastor
alejandro.pastor@alumnos.uc3m.es

Guillermo Escibano
guescrib@ing.uc3m.es

Manuel Sanjurjo-Rivo
msanjurj@ing.uc3m.es

Diego Escobar
descobar@gmv.com

¹ GMV, 11 Isaac Newton, 28670, Tres Cantos, Madrid, Spain

² Universidad Carlos III de Madrid, 30 Av. de la Universidad, Leganés 28911 Madrid, Spain